6-1-2016

Improved decoder metrics for DS-CDMA in practical 3G systems

Shady Osama Mahmoud Elbassiouny

THE AMERICAN UNIVERSITY IN CAIRO
الجامعة الأمريكية بالقاهرة
SCHOOL OF SCIENCES AND ENGINEERING

MASTER THESIS

Improved decoder metrics for DS-CDMA in practical 3G systems

A Thesis Submitted to

Electronics and communications engineering department

In partial fulfillment of the requirements for the degree of Master of Science

By: Shady Osama Mahmoud ElBassiouny

Supervisor: Prof. Ayman Elezabi

Cairo, February 2016

ABSTRACT

While 4G mobile networks have been deployed since 2008. In several of the more developed markets, 3G mobile networks are still growing with 3G having the largest market -in terms of number of users- by 2019 [1]. 3G networks are based on Direct- Sequence Code-Division Multiple-Access (DS-CDMA). DS-CDMA suffers mainly from the Multiple Access Interference (MAI) and fading. Multi-User Detectors (MUDs) and Error Correcting Codes (ECCs) are the primary means to combat MAI and fading. MUDs, however, suffer from high complexity, including most of sub-optimal algorithms. Hence, most commercial implementations still use conventional single-user matched filter detectors. This thesis proposes improved channel decoder metrics for enhancing uplink performance in 3G systems. The basic idea is to model the MAI as conditionally Gaussian, instead of Gaussian, conditioned on the users' cross-correlations and/or the channel fading coefficients. The conditioning implies a time-dependent variance that provides enhanced reliability estimates at the decoder inputs. We derive improved log-likelihood ratios (ILLRs) for bit- and chip- asynchronous multipath fading channels. We show that while utilizing knowledge of all users' code sequences for the ILLR metric is very complicated in chip-asynchronous reception, a simplified expression relying on truncated group delay results in negligible performance loss. We also derive an expression for the error probability using the standard Gaussian approximation for asynchronous channels for the widely used raised cosine pule shaping. Our study framework considers practical 3G systems, with finite interleaving, correlated multipath fading channel models, practical pulse shaping, and system parameters obtained from CDMA2000 standard. Our results show that for the fully practical cellular uplink channel, the performance advantage due to ILLRs is significant and approaches 3 dB.

ACKNOWLEDGEMENTS

الحمد لله الذي تتم بنعمته الصالحات

Firstly, I would like to express my sincere gratitude to my advisor Prof. Ayman Elezabi for the continuous support of my M.Sc study and related research, for his patience, motivation, and immense knowledge. His guidance helped me in all the time of research and writing of this thesis. I could not have imagined having a better advisor and mentor for my MSc. study.

Besides my advisor, I would like to thank the rest of my thesis committee: Dr. Karim G. Seddik, and Dr. Ayman M. Hassan, for their insightful comments and encouragement, but also for the hard questions, which motivated me to widen my research from various perspectives.

I thank my fellow colleagues and friends at the AUC for being by my side at all times. Also I thank my co-workers at AvidBeam for their understanding of the times I had to take breaks in order to focus on my thesis work.

Last but not the least, I would like to thank my family, my parents and to my brother for supporting me spiritually throughout writing this thesis and my life in general. I am thankful to everyone who motivated me in order to accomplish my MSc. studies.

TABLE OF CONTENTS

1. LITERATURE REVIEW 1

CDMA Transmission & detectors 2

Channel Encoding in 3G Systems 7

3G Standards 10

CDMA2000 vs. WCDMA 11

Some of the Similarities [19] 11

Some of the Differences 12

Detailed Comparison 13

Summary Comparison 19

2. IMPROVED LLRS 20

Problem Statement 21

MAI Variance Formulation 21

Synchronous Reception 22

Chip Synchronous and Bit Asynchronous Reception 29

3. ASYNCHRONOUS RECEPTION 33

Chip Asynchronous and Bit Asynchronous Reception 34

RC Pulse Shaping 41

MAI Variance with RC pulse Shape 48

Synchronous Reception 53

Asynchronous Reception 54

BER Performance for Synchronous and Asynchronous Reception 55

4. PERFORMANCE COMPARISON FOR ASYNCHRONOUS MULTI-PATH CHANNELS 60

Simulation Parameters 61

Turbo Decoders 63

Channel modelling 64

Single-Path channel 64
Multi-Path channel 65
Receiver Structure 65
Rake Receiver 65
Generalized Rake 66
Simulation Results 66
Modified SGA based on the pulse shape 66
Varying Truncated Group Delay 67
Multi-path 69
Additional simulation results 73
5. CONCLUSION 74
Bibliography 76
Appendix 80

TABLE OF FIGURES

Figure 1: Spreading Concept [2] 3
Figure 2: System Block Diagram 3
Figure 3: Multi-stage Interference Cancellation [7] 6
Figure 4: WCDMA encoder structure [17] 8
Figure 5: CDMA 2000 turbo encoder [38] 9
Figure 6: CDMA 2000 Pilot Channel 14
Figure 7: WCDMA Pilot Channel 15
Figure 8: CDMA2000 Synchronous timing 16
Figure 9: WCDMA asynchronous timing 16
Figure 10: CDMA2000 Reverse channels 18
Figure 11: RX Sequence of user of interest 21
Figure 12: RX from two synchronous users 22
Figure 13: ILLR BER for Bit synchronous reception 27
Figure 14: Correlated fading vs. uncorrelated fading for TBS = 2298 and Doppler 850 Hz 28
Figure 15: Correlated fading vs. uncorrelated fading for TBS = 20730 and Doppler 200 Hz 29
Figure 16: RX of chip synchronous users 30
Figure 17: ILLR BER for Chip synchronous reception 32
Figure 18: RX of asynchronous users 35
Figure 19: Interfering bits 37
Figure 20: TX & RX RRC in a system [26] 41
Figure 21: RC Time Response with β a parameter 42
Figure 22: RC Frequency Response vs. β 43
Figure 23: PDF of RX(t) at shift = 0 Tc 45
Figure 24: PDF of RX(t) at shift = 0.125 Tc 45
Figure 25: PDF of RX(t) at shift = 0.25 Tc 45
Figure 26: PDF of RX(t) at shift = 0.375 Tc 45
Figure 27: PDF of RX(t) at shift = 0.5 Tc 45
Figure 28: PDF of $RX(t)^2$ at shift = 0.375 Tc 46
Figure 29: PDF of $RX(t)^2$ at shift = 0 Tc 46
Figure 30: PDF of $RX(t)^2$ at shift = 0.125 Tc 46
Figure 31: PDF of $RX(t)^2$ at shift = 0.25 Tc 46
Figure 32: PDF of $RX(t)^2$ at shift = 0.5 Tc 47

Figure 33: Maximum Value of RC against shift and varyingβ 48
Figure 34: RRC Waveform based on Random Sequence..... 49
Figure 35: P(0)..... 51
Figure 36: P(1)..... 52
Figure 37: Progressive MAI Variance after De-Spreading for K=13, N = 8 53
Figure 38: MAI after De-Spreading in chip aligned reception for different K, and N 54
Figure 39: MAI after De-Spreading in chip miss-aligned reception for different K, and N 55
Figure 40: Uncoded BER in fading channel 56
Figure 41: Variance of shifts for different roll-off factors 57
Figure 42: Sum of Raised cosine squared at β=0..... 58
Figure 43: Sum of Raised cosine squared at β=0.22..... 59
Figure 44: Sum of Raised cosine squared at β=1 59
Figure 45: The TDD frame structure 61
Figure 46: Rake receiver structure..... 66
Figure 47: BER after SGA correction for asynchronous reception..... 67
Figure 48: Worst Case Squared error vs. Truncation depth for various shifts 68
Figure 49: Varying TD on BER performance 69
Figure 50: BER for multi-path asynchronous reception..... 70
Figure 51: BER for K=10, N=16 in a 4-path correlated fading channel..... 71
Figure 52: SNR required to achieve BLER = $10-2$ for various number of users..... 72
Figure 53: Changing the coding rate effect on ILLR-XC..... 73

LIST OF TABLES

Table 1: WCDMA vs. CDMA2000 10
Table 2: Effciency per service comparison between MC and DS [19] 12
Table 3: CDMA2000 Spreading rates [20] 13
Table 4: WCDMA Spreading rates 14
Table 5: Code comparison [18] 18
Table 6: CDMA2000 vs WCDMA 19
Table 7: Chip aligned and Chip misaligned MAI for Rectangular pulses [23] 53
Table 8: Correction term for BER in fading channel 55
Table 9: 4 Path delays and Path gains 70

LIST OF NOTATIONS

σ	Variance
β	Raised Cosine/Square Root Raised Cosine roll off factor
$E[.]$	Mean
N	Spread Factor
K	Number of Users
N_s	Number of Samples in a frame
N_b	Number of Bits in a frame
L	Number of Paths
G	Group Delay
G_T	Truncated Group Delay
N_d	Integer Chip Delay
τ	Leading Fractional Chip Delay
y_1	Received signal from user 1
y_{1d}	Received signal from user 1 after de-spreading
ζ	The received signal from MAI

LIST OF ACRONYMS

SNR	Signal-to-Noise Ratio. The ratio of the average received modulated carrier power to the noise power (typically thermal noise modelled as Additive White Gaussian Noise (AWGN). It is measured in dB.
RC	Raised Cosine Pulse
RRC	Square Root Cosine Pulse
ISI	Inter Symbol Interference
SLL	Side Lobe Level
MC	Multi-Carrier
DS	Direct Spread
MS	Mobile Station
PN	Pseudo Noise
OVSF	Orthogonal Variable Spreading Factor
MRC	Maximum Ratio Combining
EGC	Equal Gain Combining
GR	Generalized Rake
CR	Code Rate
TBS	Transport Block Size
MF	Matched Filter
TD	Truncation Depth
MAI	Multiple Access Interference
MLSD	Maximum Likelihood Sequence Detection
MUD	Muti-User Detector
MAP	Maximum Aposteriori Detecor
IC	Interference Cancellation
PIC	Parallel Interference Canceller
SIC	Sequential Interference Canceller
PCCC	Parallel Concatenated Convolutional Code
RSC	Recursive Systematic Constituent
LLR	Log Likelihood Ratio

CHAPTER 1

1. LITERATURE REVIEW

CDMA Transmission & detectors

The Direct Sequence Code Division Multiple Access (DS-CDMA) basic concept is to multiply the low rate baseband signal (having low bandwidth) with a high rate spreading code. This multiplication leads to an increase in bandwidth of the transmitted signal; as the transmitted signal will now occupy the bandwidth corresponding to the high rate spreading sequence. At the receiver, the counteraction is done which is called De-Spreading: that is to re-multiply the received sequence with the conjugate of the initial spreading sequence (Both the TX and the RX know the spreading sequence with prior negotiation), this results in the recovery of the original low rate baseband sequence. Spreading the low rate sequence causes the message to be spread in the frequency domain over higher bandwidth making the original sequence underlie the noise floor level, this feature is a desired by-product of spreading; as the communication now is secure and appear as a random noise at any receiver not having the spreading sequence.

In the time domain, the spreading causes the interference power to be spread over different chips (where each bit is spread with multiple chips). This spreading smoothen the interference on the desired bit stream. Figure 1 is an illustration of the spreading concept, in which, the low rate sequence is spread in the frequency domain to a higher bandwidth occupancy, channel noise is added to the TX symbols, and the rest of the users in the system appear as an interference occupying the same bandwidth. After De-Spreading, the message signal is shrunk in bandwidth again and rises above the noise level once more for proper reception. The codes used for spreading the data are chosen to be orthogonal such that the integration of these codes over a bit interval should give exactly zero to avoid intentional interference.

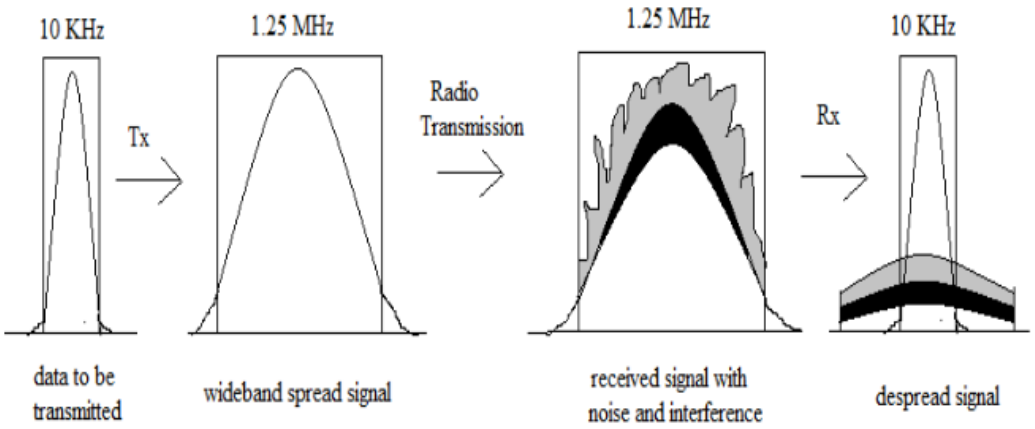

Figure 1: Spreading Concept [2]

The DS-CDMA system model is shown below

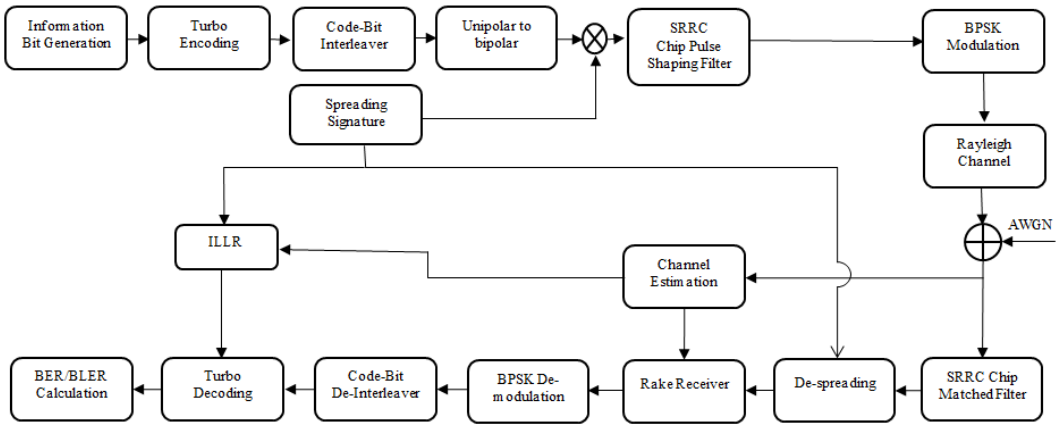

Figure 2: System Block Diagram

The system starts by generating random information bits that are composed of ones and zeros, these bits form a code-word. Each code-word is acted upon by the turbo encoder with a resulting bit stream equal to $1/CR$ (where CR is the code rate of the turbo encoder) and some tail bits for the encoder termination. Multiple code-words form a frame which in turn is interleaved (interleaving on the frame level) before being modulated. BPSK modulation is done and spreading is performed to the interleaved bits. For the simulation sake, encoding is only performed on the user of interest (User 1), while randomly generated symbols are used for the interfering users. After modulation is done, the sequence is then passed through a transmit filter, the filter can be a rectangular pulses filter or the

RRC filter. We are interested in the RRC pulse shapes because it is the one implied by the standard.

After shaping of the code bit sequence, the received signal from users are passed through a Multi-path Rayleigh fading channel with delays set based on the simulation of interest. The total delay between the user of interest and the interfering user is the summation of the path delay and the user delay.

After passing through the multipath Rayleigh fading channel, an AWGN is added to the faded signal. The noise is normalized based on the number of paths, spread factor, code rate, up sampling factor, SNR. The receiver branch is the complementary of the transmitter branch. MF is used at the receiver followed by BPSK demodulation, code-bit interleaver, Turbo decoder, and finally BER calculation. The Turbo decoder is fed by the LLR/ILLR values discussed earlier for soft bit decoding.

The CDMA systems are not noise-limited. At high SNR, an increase in the signal to noise ratio will not cause any improvement in the system performance (measured in bit error rate or frame error rate). CDMA systems are therefore classified as interference-limited [3]; as introducing one or more interfering users causes the system to saturate, this is of course given a constant spreading factor, i.e. CDMA system capacity is limited by the number of interfering users not by the signal to noise ratio [4], [5]. The system capacity depends on the number of unique sequences that can be assigned to different users. In reality, the reception of these spreading sequences (codes) is usually not completely orthogonal, and there exists a weak cross correlation between these codes at the reception causing Multiple Access Interference (MAI). If the number of users in the systems is high (valid assumption in real systems), then the interference can be modeled as a Gaussian noise in the background “using the central limit theorem”. The receiver in turn is composed of a bank of chip Matched Filters (MF) [6]. These filters are matched to the signature sequences.

Although the MAI can be approximated as AWGN, it consists of received signals of CDMA users. Thus, MAI is very structured, and can be taken into consideration in the receiver. This leads [7] to analyze the optimal multi-user detectors (MUDs) for

DS-CDMA communications. It was shown that the CDMA systems are not interference limited by nature, but the conventional matched filter (MF) receiver had its limitations. The optimal MUDs can be Maximum Aposteriori (MAP) detector or Maximum Likelihood Sequence Detection (MLSD). These techniques are also used in combating inter-symbol interference. However, MAP and MLSD have an exponential implementation complexity as a function of the number of users in the system. This complexity paved the way for many published papers for sub-optimal multi-user detectors, some of the sub-optimal multi-user detectors are discussed in [8].

The sub-optimal MUDs can be classified in many ways: One way of classification is centralized/decentralized single user detection techniques. The centralized algorithms does true multi-user joint detection; they can detect all the users' data symbols. The decentralized algorithms detect a single user data symbols based on the received signal of a multi-user environment containing MAI. The centralized algorithms can be used in base station receiver implementation, while the single user-based receivers can be used in both the base station receivers and the mobile users' receiver.

Another classification method is based on the method applied to the multi-user and single user detectors. Linear equalizers and the subtractive interference cancellation are the two most known variants of this category. Linear equalizers are essentially linear filers that are used to suppress noise and the MAI, the two most known linear equalizers are the Zero Forcing (ZF) detector, and the Minimum Mean Square Error (MMSE) detector. The MMSE detector can work with training sequences (Pilots), or can work in a blind equalization fashion. On the other hand, the subtractive interference cancellers can be classified as Parallel Interference Cancellers (PIC) [9], or Sequential Interference Cancellers (SIC). Both cancellers tries to estimate the MAI and subtracts its effect on the received sequence in attempt of better decoding performance. The PIC can work on all users at the same time so it is ideal to operate with centralized MUDs. The SIC mode of operation is to estimate the interference of the users and sequentially subtract their effect. It is worth noting that both Linear and IC equalizers can be used in centralized receivers, while linear equalizers can be implemented

adaptively in such a way that can be used for single user decentralized detectors. This is only possible if the spreading sequences are repeated on the bit level i.e. the MAI becomes cyclo-stationary.

The PIC are considered the most suitable decoders to be applied in a CDMA system in the base station design. An implementation of the PIC is shown in Figure 3. Initial estimates of the MAI can be re-used in a multi-stage interference cancelation scheme. As the number of the stages increase, the confidence in the decisions increase but at the expense of a delay in detection.

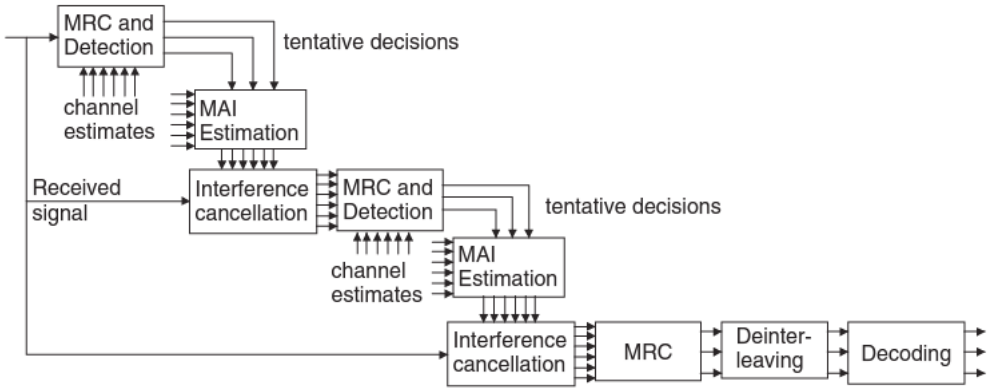

Figure 3: Multi-stage Interference Cancellation [7]

Multi-user detectors and error-control coding are two primary means to improve performance of DS-CDMA in wireless systems. Little interest has been given to the single-user decoder metrics, however. Examples of such works include [10] who showed that reliable MAI variance estimation can improve the decoding process. [11] [12] [13] have also utilized the single decoder metrics for enhanced parallel interference cancellation. Despite such progress in the research arena, implementation in commercial products lagged significantly, with most deployed chipsets implementing the conventional matched filter. This was partly due to the high complexity of even sub-optimum multiuser detectors. One of the highly publicized parallel interference cancellers appeared in 2008 [14]. As for improved decoder metrics, the authors are not aware of any commercial implementation. The fundamental idea behind improved decoder metrics is to model the MAI rather than assume it is Gaussian. The method employed in [15] is to model the MAI as conditionally Gaussian, where the conditioning may be on the user cross-

correlations, the interfering user channels, or both. All this information is available, or must be obtained, at the base station receiver. This results in the MAI plus Noise (MAIN) being modeled as Gaussian with a time-dependent variance, and results in performance gains compared to decoders using the conventional metric, which makes the well-known standard Gaussian Approximation (SGA).

The work in [13]was based on parallel interference cancellers (PIC) In this paper we propose improved Log-Likelihood Ratios (LLR's) for matched filter detectors, which we believe is still the most widely deployed implementation. Because of the inferior performance of matched filter detectors, the gains to be had with ILLR are significantly larger.

Channel Encoding in 3G Systems

Channel codes are used to enhance the BER performance of mobile systems by providing enough redundancy in bits that allow detection and correction of bit errors caused by the wireless channel. The turbo codes are one of the most robust techniques that enhances the error correction capabilities in wireless systems. Turbo codes are used in 3G mobile standards (UMTS, and CDMA2000).

The turbo codes lie under the umbrella of Forward-Error-Correcting (FEC) codes. FEC codes basic concept is that k bits enter the encoder, while the encoder produces n output bits where k<n. Out of 2^n output bit combinations only 2^k are only allowable. This provides the capability to detect and even correct bit errors. The k/n ratio is referred as the code rate. Lower code rates result in better error correction and this better energy efficiency. However, this decreases the bandwidth efficiency. This is why choosing a suitable code rate is a design trade-off. The standard might also allow different coding rates depending on the instantaneous channel conditions to better balance between energy and bandwidth efficiencies.

The turbo codes were introduced by French researchers back in 1993 [16]. The introduction of the turbo codes was indeed a breakthrough at its time. A performance only half a dB away from the Shannon channel capacity was

attainable using the turbo codes; this lead to its adoption in many applications and standards.

The encoder structure used by 3GPP in WCDMA standard is shown in Figure 4.

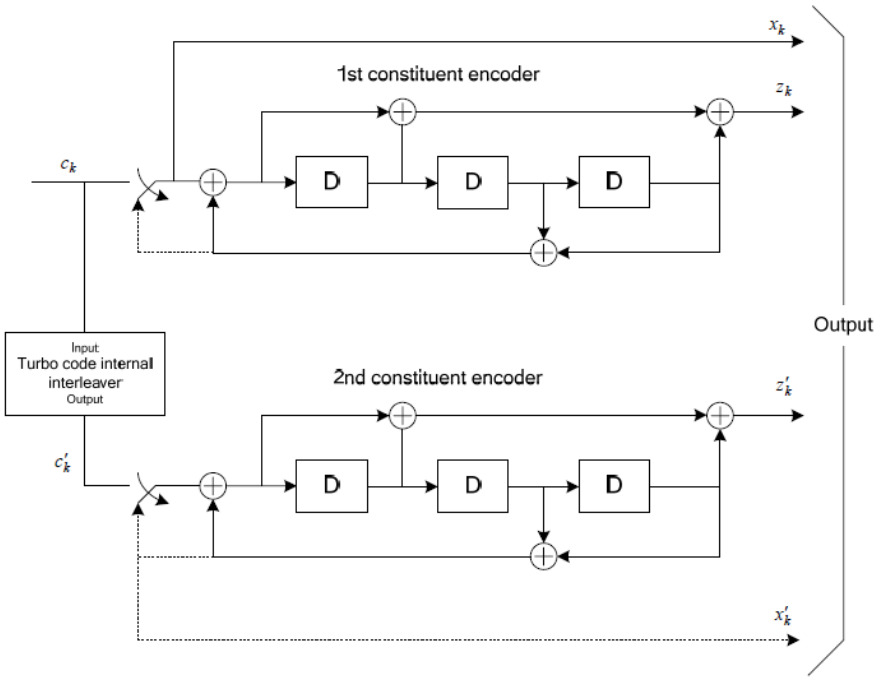

Figure 4: WCDMA encoder structure [17]

The encoder structure is composed of three output code bits (x_k, z_k, z_k') for each single input bit. The encoder structure is composed of two identical recursive systematic convolutional (RSC) encoders that are separated by an internal interleaver that is used to change the order of the bits entering the second constituent encoder. It should be noted that the WCDMA turbo encoder does not take care of different coding rates, the only possible coding rate is $\frac{1}{3}$.

The transfer function of the 8-state constituent code for the Parallel Concatenated Convolutional Code (PCCC) is :

$$G(D) = \left[1, \frac{g_1(D)}{g_0(D)}\right], \text{ Where } g_0(D) = 1 + D^2 + D^3, g_1(D) = 1 + D + D^3.$$

The CDMA 2000 turbo encoder is not that different from the WCDMA encoder, it also uses two RSC encoders but with a different transfer function. The CDMA 2000 turbo encoder is shown in Figure 5.

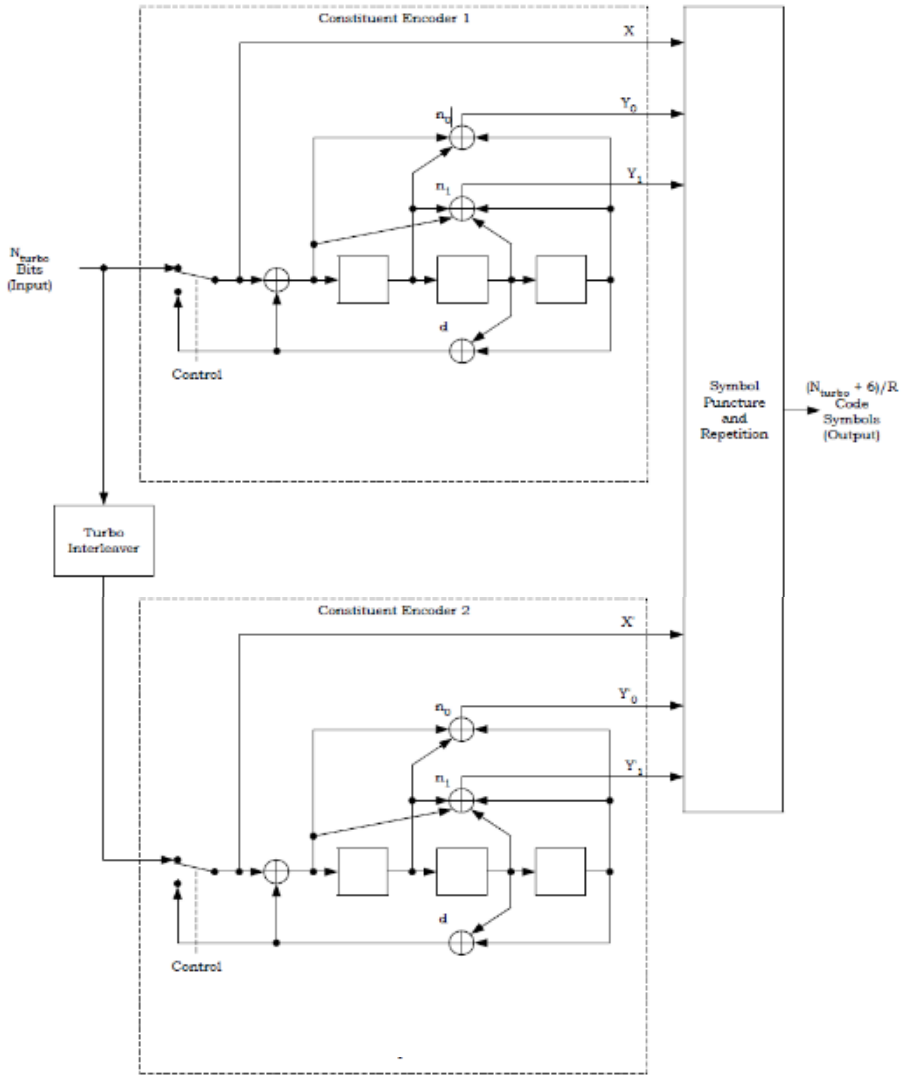

Figure 5: CDMA 2000 turbo encoder [38]

The CDMA 2000 turbo encoder transfer function is given by

$$G(D) = [1 \quad \frac{n_o(D)}{d(D)} \quad \frac{n_1(D)}{d(D)}], \text{ Where } d(D) = 1 + D^2 + D^3, n_o(D) = 1 + D + D^3, \text{ and}$$

$$n_1(D) = 1 + D + D^2 + D^3$$

The CDMA 2000 turbo encoder can support multiple code rates depending on the output selected from the six output code bits. The supported rates are $\frac{1}{2}, \frac{1}{3}, \frac{1}{4}, \frac{1}{5}$.

Puncturing of code bits are done after encoding to accommodate for the different possible code rates. It is worth noting that the Bit error rate performance of the CDMA 2000 encoder and the WCDMA encoder are very close to each other for the same coding rate.

3G Standards

After covering the core aspects in CDMA physical layer design, we will cover the different standardized 3G technologies and compare them side by side.

Although the CDMA concept was developed during the 1960's, 3G technologies first appeared at the beginning of the new century due to advancements in computation capabilities in hand-held devices. 3G networks depend on Code Division Multiple Access Technique. The main two standards under the umbrella of 3G technologies are UMTS (W-CDMA) and CDMA 2000. Table 1 describes some of the differences of the two systems.

Table 1: WCDMA vs. CDMA2000

FEATURE	UMTS (3GSM)	IS-2000 (CDMA 2000)
TECHNOLOGY	W-CDMA	CDMA
GENERATION	3G	3G
ENCODING	Digital	Digital
YEAR OF FIRST USE	2001	2000 / 2002
ROAMING	Worldwide	Limited
HANDSET INTEROPERABILITY	SIM card	RUIM (rarely used)
COMMON INTERFERENCE	None	None
SIGNAL QUALITY/COVERAGE AREA	Smaller cells and lower indoors coverage on 2100 MHz; equivalent coverage indoors and superior range to GSM on 850/900 MHz.	Unlimited cell size, low transmitter power permits large cells
FREQUENCY UTILIZATION/CALL DENSITY	5 MHz = 2 Mbit/s. 42Mbit/s for HSPA+. Each call uses 1.8-12 kbit/s depending on chosen quality and audio complexity.	1.228 MHz = 3Mbit/s
HANDOFF	Soft	Soft
VOICE AND DATA AT THE SAME TIME	Yes	No EVDO / Yes SVDO

Both standards had similar objectives; they wanted to satisfy certain technology needs. The main objectives of the 3G technologies are [18]

1. IP access to the world wide web (Internet)
2. Higher Bandwidth
3. Wider range of applications
4. Higher Data rates
5. 2 Mbps in low mobility
    a. 384 kbps in open spaces
    b. 144 kbps in high mobility
    c. Co-existence with 2G networks
6. International roaming services between different operators
7. Different services based on the channel quality
8. High Spectral efficiency
9. Services based on geographical location
10. Services based on user profile

CDMA2000 vs. WCDMA

Some of the Similarities [19]

1. Coherent Uplink and Downlink
2. Fast Power Control in Uplink and Downlink
3. Variable length Orthogonal Walsh sequences channel codes for uplink and downlink to separate users
4. Variable Spreading factor for higher data rates and blind rate estimation for simple services.
5. Turbo Codes for high data rates
6. Convolutional codes for low data rate
7. Complex QPSK Spreading in the downlink
8. Soft handoff and mobile assisted inter-frequency hard handoff
9. Same pulse shape factor in the TX of Square Root Raised Cosine (RRC) with roll-off factor = 0.22

Some of the Differences

1. Both CDMA2000 and WCDMA uses Direct Spread (DS) in the channel structure, however, CDMA2000 additionally uses Multicarrier (MC) CDMA technique to:
    a. Achieve similar performance compared to conventional single carrier
    b. Backward compatibility with IS-95

    The efficiency comparison between MC and DS is illustrated in the table below

Table 2: Effciency per service comparison between MC and DS [19]

Service	Environment	Spectrum Efficiency (RL/FL) (users/MHz/cell) for voice (Mbps/MHz/cell) for data	
		Multicarrier (MC)	*Direct Spread (DS)*
Voice 9.6 kbps 1% FER	***Vehicular***	29 / 28.2	29 / 45.1
	Pedestrian	42.1 / 45.8	43.2 / 45.3
	Indoor	38.9 / 32.5	34.7 / 33.6
	Mixed	34.1 / 34.6	35.7 / 46.1
Packet Data 76.8 kbps 10% FER	*Vehicular*	0.176 / 0.094	0.209 / 0.138
	Pedestrian	0.253 / 0.099	0.264 / 0.111
	Indoor	0.218 / 0.064	0.226 / 0.070

2. Chip rates: CDMA 2000 uses 3.6864 Mcps while WCDMA uses 3.84 Mcps WCDMA has power control at rate 1600 Hz while CDMA 2000 uses 800 Hz, other than that their open loop and closed loop power control systems are similar.
3. Frame lengths
    a. CDMA 2000

    20 ms for data and control and 5 ms for control information on control channels

    b. WCDMA

10ms/20ms (optional)

- 5 and 10 ms are appropriate for low-delay data applications
- 20 ms frame length is considered the base for voice and data applications with overhead being 11% instead of 20% in 10 ms frames.

4. Spreading

a. CDMA 2000

- Variable length Walsh sequence for channel separation and M-sequence with length 2^{15} in the downlink
- Variable length orthogonal sequences, M-sequence 2^{15} and 2^{41} for user separation

b. WCDMA

- Variable length orthogonal sequence for channel separation and Gold sequence with length 2^{18} for cell and user separation in the downlink
- Variable length orthogonal sequences, M-sequence 2^{15} and 2^{41} for user separation

Detailed Comparison

Spreading rates

- CDMA 2000

The spreading rates are calculated as N*1.2288 Mcps where N can takes values 1, 3, 7, 9, 11. The supported bandwidths in CDM2000 are 1.25, 3.75, 7.5, 11.5, 15 MHz. The mapping between the bandwidth and its corresponding spreading rate is summarized in Table 3.

Table 3: CDMA2000 Spreading rates [20]

BANDWIDTH (MHZ)	SPREADING RATE (MCPS)
1.25	1.2288
3.75	3.6864
7.5	7.3278
11.5	11.0952
15	14.7456

The choice of these spreading rates to ensure backward compatibility with IS-95B.

- WCDMA

Table 4: WCDMA Spreading rates

BANDWIDTH (MHZ)	SPREADING RATE (MCPS)
5	4.096
10	8.192
20	16.384

Pilot Channels

Pilots are used as reference signals for channel estimation, time synchronization, phase synchronization, system acquisition, and help in coherent demodulation.

- CDMA2000

In CDMA2000 the Pilot channel is shared between the different Mobile Stations (MS) in the forward link as shown in Figure 6. The pilot channel is code-multiplexed using Walsh codes for orthogonal spreading. In the reverse link pilot signals are time multiplexed and are dedicated to each user.

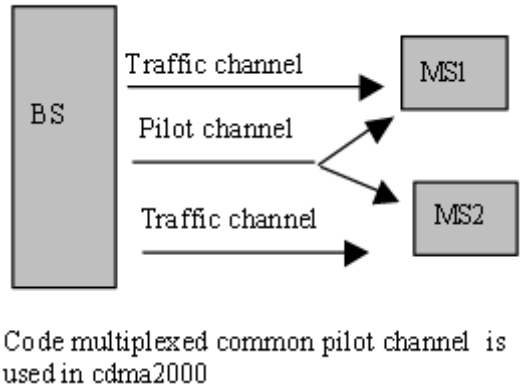

Figure 6: CDMA 2000 Pilot Channel

- WCDMA

In WCDMA the Pilot channel is time multiplexed with the traffic channel, each traffic frame contains a number of pilot bits as shown in Figure 7.

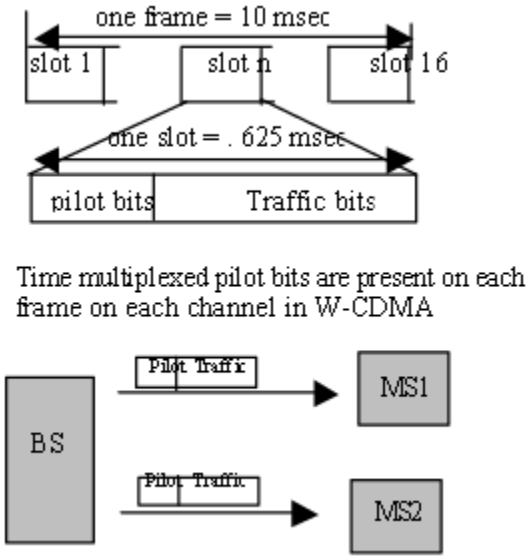

Figure 7: WCDMA Pilot Channel

Synchronous vs. asynchronous cells

- CDMA 2000

CDMA operates in synchronous mode; in which the transmission and reception time of the cells are synchronized. The system uses a common timing source such as the Global Positioning System (GPS) as shown in Figure 8, the cells transmit a PN sequence of length 2^{15}-1 chips with periodicity of 26.67 milliseconds. The sequence is sent from different base stations using different time offsets of multiples of 64 chips to provide cell distinction. The time synchronization assists in soft hand-off between cells.

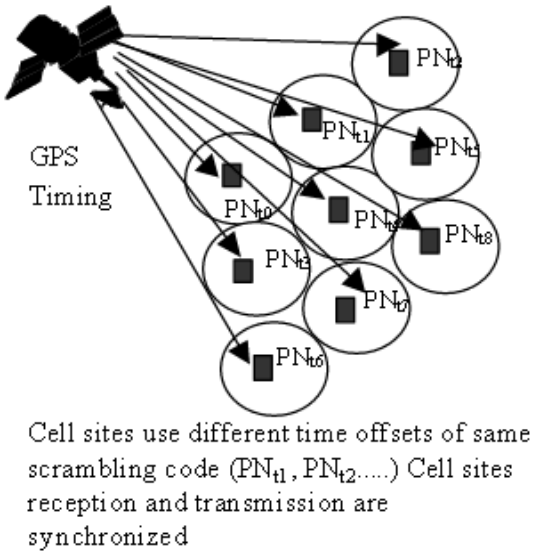

Figure 8: CDMA2000 Synchronous timing

- WCDMA

In WCDMA the cell transmission and reception are not synchronized, but instead each cell uses a unique scrambling code (compared to the same PN sequence with different time offset as in the case of CDMA 2000) to uniquely identify the cell. These codes are 40,960 chips in length and are transmitted every 10 ms. The asynchronous cell structure is shown in Figure 9.

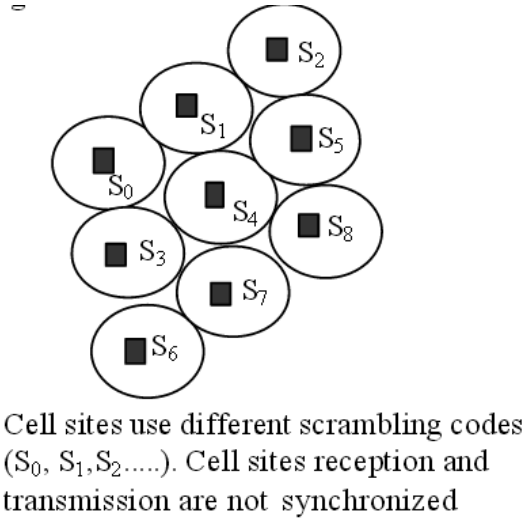

Figure 9: WCDMA asynchronous timing

Channels

- WCDMA
  1. Transport Channels
     a. Dedicated Channels
     b. Common Channels
        i. BCH
        ii. FACH
        iii. PCH
        iv. RACH
        v. CPCH
        vi. DSCH
        vii. HS-DSCH
  2. Physical Channels

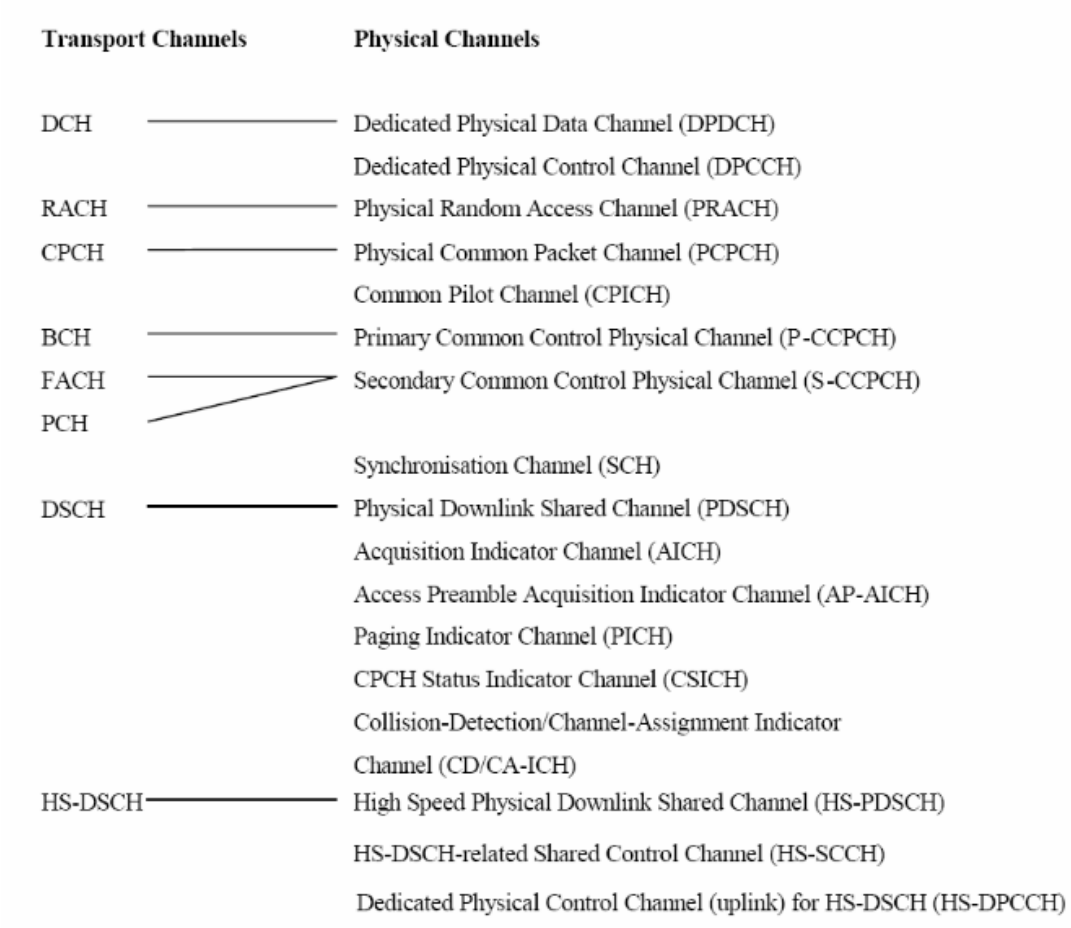

  3. Logical Channels
  4. Shared Channels

- CDMA2000

Reverse channel

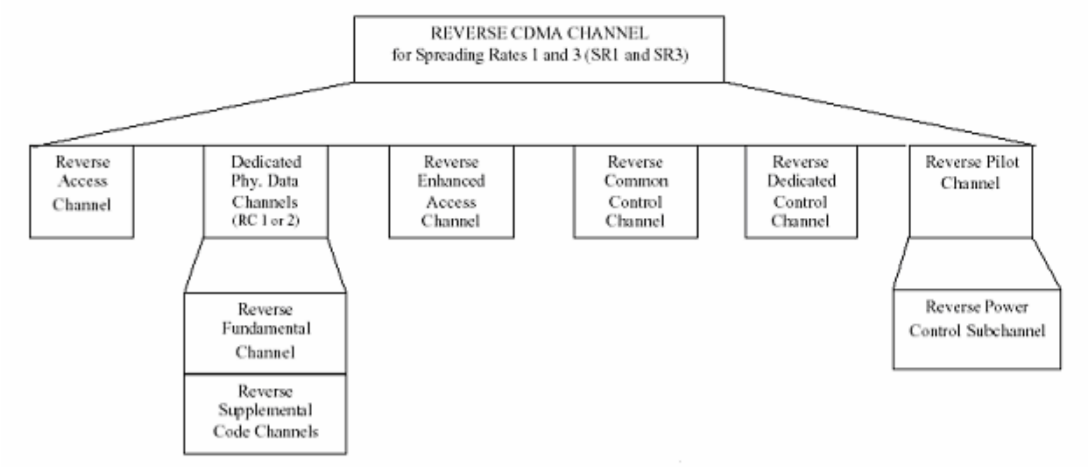

Figure 10: CDMA2000 Reverse channels

Codes

The Codes used in the CDMA systems can be classified into

1) Codification Codes
    a. Orthogonal Codes (Synchrony Codes)
    b. Pseudo noise Codes (PN Codes)
2) Canalization Codes
3) Scrambling Codes

They differ in the directions they are used in (Uplink/Downlink), their Auto-Correlation and Cross-Correlation characteristics, .. etc. An example of the different usage of each type of codes is given in Table 5.

Table 5: Code comparison [18]

	Synchrony Codes	**Canalization Codes**	**PN Codes (Uplink)**	**Scambling Codes (Downlink)**
Type	Gold Codes	OVSF (Walsh Codes)	Gold codes and S-Codes	Gold Codes
Length	256 Chips	4-512 Chips	38400-256 Chips	38400 Chips
Period	66.27 μs	1.04-133.34 μs	10 ms-66.67 μs	10 ms

Code Number	1 Primary/ 16 Secondary	4-256 (Uplink) 4-512 (Downlink)	16,777,216	512 Primary/15 Secondary
Spreading	No	Yes	No	No

Summary Comparison

A comparison between CDMA 2000 and WCDMA is summarized inTable 6 [21].

Table 6: CDMA2000 vs WCDMA

Parameters	W-CDMA	CDMA2000
Multiple access technique	DS-CDMA	Uplink DS-CDMA Downlink MC-CDMA/DS-CDMA
Chip rate	3.84 Mcps	N x 1.2288 Mcps Where N = 1, 3, 6, 9, 12
Modulation Scheme	Uplink Dual channel QPSK; Downlink QPSK	Uplink: BPSK; Downlink: QPSK
Frame Length	10 ms with 15 slots	5, 10, 20, 40, 80 ms
Pilot Structure	Dedicated pilots on the uplink and common or dedicated pilots on the downlink	Uplink Code-divided continuous dedicated pilot Downlink Code-divided continuous common pilot and dedicated or common auxiliary pilots
Spreading Modulation	QPSK both directions	Uplink M-ary PSK Downlink QPSK
Detection	Coherent pilot aided	Coherent pilot aided
Scrambling codes	Uplink Short code (256 chips) or long code (38,400 chips Gold code) Downlink Gold code	Long code ($2^{42} - 1$ chips) Short code ($2^{42} - 1$ chips)
Channelization codes	Orthogonal Variable Spreading factor (OVSF) codes	Uplink Walsh codes Downlink Walsh or quasi-orthogonal codes
Inter-cell site operation	Asynchronous Synchronous (optional)	Synchronous
Pulse shape	RRC with β=0.22	RRC with β=0.22
Voice Coder	EVRC	ACELP
TBSs	40-6144 (188 Possible Values)	384-36864 (12 Possible Values)

CHAPTER 2

2. IMPROVED LLRS

Problem Statement

The interference experience by users in CDMA systems are affected by the chip pulse shape characteristics used in the CDMA system standard. Better identification of the pulse shape effect on the MAI characteristics can better describe the bit LLR which is fed to the decoder and thus better BER performance. The better BER performance is a result of better identification of the weakly interfered bits and the strongly interfered bits.

MAI Variance Formulation

When studying the effect of Multiple Access Interference (MAI) we will consider a single interfering user with only a single path. The study can then be generalized. There are three possible interference patterns than can occur in CDMA

1) Chip and Bit Synchronous Interference
2) Chip Synchronous and Bit Asynchronous Interference
3) Chip Asynchronous Interference

These three modes will be studied in depth. The system model is illustrated in the figure bellow:

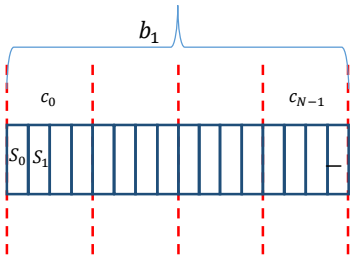

Figure 11: RX Sequence of user of interest

The user of interest has a stream sequence of bits b_k where k denotes the k^{th} bit, these bits are spreaded using a spreading sequence. The number of chips per chip is the spread factor N. The chip is then transmitted through a pulse shaping filter to be transmitted. The pulse shape is a continuous time waveform; however, for the sake of simulations the pulse shape is discretized in samples s, where the number of samples per chip is called the Up Sampling Factor (USF).

The received signal after despreading in synchronous reception can be expressed as

$$y_{1g} = |h_1|^2 b_{1,g} + \sum_{j=2}^{K} \sum_{i=g.N}^{g.N+N-1} b_{j,g} |h_j||h_1| \cos(\theta_j - \theta_1)\, c_{1,i} c_{j,i} + n_1$$

Equation 1

where g is the bit index, K is the number of users, $b_{j,g}$ is the bit of user j and index g, h_j is user's j complex channel coefficient, $c_{j,i}$ is the user's j chip i, and n_1 is the AWGN.

Synchronous Reception

The pulse shape is confined within the chip period T_c

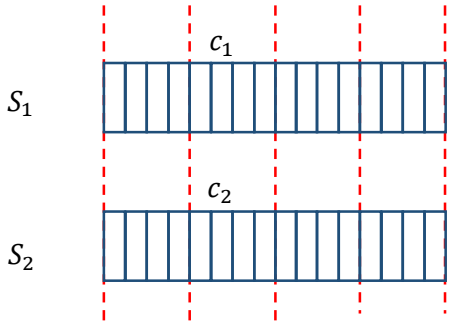

Figure 12: RX from two synchronous users

The received signal can be written as

$$y_1 = b_1 c_{1i} + b_2 c_{2i}$$

After passing through the matched filter the output is then sampled at the sampling instants m where $m = 0,1,2,3\ T_c$. In most pulse shapes, the pulse shapes are chosen to have zero crossings at the multiples of T_S, hence the inter-symbol interference is zero. For synchronous reception, the interference on the chips is based on aligned interfering users which will be resulting from the interfering users chips at the sampling instants. The values at these instants are the maximum attainable within the pulse shape.

After de-spreading the resulting received signal can be expressed as

$$y_{1g} = \sum_{i=0}^{N-1} (b_1 c_{1i} E_c + b_2 c_{2i} E_c)\, c_{1i}^*$$

Where E_c is the energy per chip. It should be noted that $E_b = N.E_c$ and we operate at $E_b = 1$. Also, $\sum_{i=0}^{N-1} c_{1i}c_{1i}^* = N$. Given these two facts the previous equation can be simplified to:

MAI

$$y_{1g} = b_1 + b_2.\frac{1}{\mathrm{N}}\sum_{i=0}^{N-1} c_{2i}c_{1i}^*$$

The MAI variance is calculated as $E[\left(b_2.\frac{1}{\mathrm{N}}\sum_{i=0}^{N-1} c_{2i}c_{1i}^*\right)^2]$

$$\eta^2 = E\left[\left(b_2.\frac{1}{\mathrm{N}}\sum_{i=0}^{N-1} c_{2i}c_{1i}^*\right)^2\right] = E\left[\frac{b_2^2}{N^2}\right]E\left[\left(\sum_{i=0}^{N-1} c_{2i}c_{1i}^*\right)^2\right] = \frac{1}{N^2}r_{12}^2$$

Equation 2

where $r_{12}^2 = \left(\sum_{i=0}^{N-1} c_{2i}c_{1i}^*\right)^2$

It is obvious that the MAI is a function of the users cross correlations, also the MAI variance depends on the channel coefficients. The previous two factors will lead to improved LLRs that are discussed next.

In practical CDMA systems, long spreading sequences are used, which results in cross-correlations that appear random from bit to bit. The Standard Gaussian Approximation (SGA) is the conventional model used for MAI both for error probability computations as well as for computing the LLRs for the single-user decoders. This model assumes a sufficient number of users K and/or a large spreading factor N for the MAI to be well-modeled as Gaussian by the central limit theorem. Specifically, a large N will result in each interfering user contribution being approximately Gaussian, and a large K will result in the MAI to be approximately Gaussian. The assumption of large K is not always valid, depending

on the number of active users. On the other hand, the spreading factor in practical systems is usually large, except when the required data rate is high, in which case the spreading factor becomes small, since the chip rate is a fixed system parameter by virtue of the fixed channel bandwidth in 3G systems. For bit- and chip-synchronous transmissions, the SGA MAI variance seen –in a Single path/Multi-path scenario- by path m of user j can be expressed as:

$$\eta_{jm}{}^2 = \frac{1}{2N}\sum_{k=1}^{K}\sum_{p=1}^{L} E_{kp} + \sigma^2 \qquad p \neq m \quad at \;\; k = j$$

Equation 3

where E_{kp} expresses the average energy per bit per path of user k path p, and σ^2 is the AWGN variance. Note that the terms where k=j are self-interference terms. The above expression can be simplified if the users have equal energies as shown below

$$\eta_{jm}{}^2 = \frac{1}{2N}\sum_{p\neq m} E_{jp} + \frac{(K-1)E_b}{2N} + \sigma^2$$

Equation 4

where E_b is the energy per code bit for all paths of each user. The equal average energy is satisfied in practice via the slow power control [22]. For chip-asynchronous transmissions, the interfering user contribution includes a factor that depends on the statistics of the random misalignment of chips [23].

The idea behind the proposed approach in obtaining the Log-likelihood Ratios (LLRs) is to recognize that the MAI terms consist of the product of the time-varying cross-correlations and the complex fading channel coefficients of other users. The cross-correlations may be computed since the user codes are known to the base station, whereas the channel coefficients must be estimated anyway for coherent detection of all user signals. Thus we may condition on the known cross-correlations and/or channels and model the MAI as conditionally Gaussian. Referring to Equation 2 and considering user 1 as the user of interest, we find that once the 'randomness' in the cross-correlations $\{r_{1j}\}$ is removed by conditioning,

the remaining term is exactly Gaussian since $X_{j1} = |h_j| \cos(\theta_j - \theta_1)$ is Gaussian. Thus, the total MAI plus noise becomes a Gaussian random variable with time-dependent variance. A further improvement may be obtained by using knowledge of the channel, i.e. fading coefficients, of other users in which case the single-user decoders would be utilizing all the available information about the interfering users. In that last case we would invoke the Central-limit theorem to model the total MAI plus noise as Gaussian.

In all cases, the LLR for the Turbo decoder of user j after applying maximal-ratio combining on the Rake receiver outputs is given by

$$L_j = \sum_{m=1}^{L} \frac{2 y_{jm} |h_{jm}|}{\eta_{jm}^2}$$

Equation 5

where η_{jm}^2 is the Multiple Access Interference (MAI) plus noise variance in path m of the signal of user j, L is the total number of paths, y_{jm} is the received signal of user j for path m, and the h_{jm} complex Gaussian fading coefficient of path m of user j.

The LLR is calculated for every bit and is fed to the turbo decoder to provide soft decision output of the decoded bits.

The idea behind improved LLRs is to model the interference as conditionally Gaussian. We condition on the user cross-correlations, the channel coefficients, or both. Note that in the case of conditioning on the cross-correlations, the MAI is exactly conditionally Gaussian, whereas in the other two cases the conditional Gaussian model is a close approximation. In all cases, the variance of the MAI becomes a time-dependent variance. Following are the conditional MAIN variances used in the three forms of ILLRs.

1) ILLR-X

By conditioning on the user-path cross-correlations and averaging over the channel coefficients, the MAI plus Noise variance seen by path m of user j is given by

$$\eta_{jm}^{\ 2} = \frac{1}{2}\sum_{k=1}^{K}\sum_{p=1}^{L} r_{jm,kp}^{\ 2} E_{kp} + \sigma^2 \qquad p \neq m \quad at \ \ k = j$$

Equation 6

where $r_{jm,kp}$ is the normalized cross-correlation between user j path m and user k path p. We refer to the above metric as the ILLR-X.

2) ILLR-C

Here, we condition on the channel estimates for each user-path and average over the cross-correlations. The ILLR in this case is given by

$$\eta_{jm}^{\ 2} = \frac{1}{N}\sum_{k=1}^{K}\sum_{p=1}^{L} X_{kp,jm}^{\ 2} + \sigma^2 \qquad p \neq m \quad at \ \ k = j$$

Equation 7

where $X_{kp,jm} = |h_{kp}|\, cos(\theta_{kp} - \theta_{jm})$ is the real fading coefficient due to the MAI from user k path p that is experienced by path m of user j. In obtaining the variance of the sum, we may easily ignore the weak dependence between the cross-correlation terms [24]. We refer to this metric as ILLR-C.

3) ILLR-XC

Here, we condition on the users' cross correlations and the channel coefficients. The conditional MAIN variance is therefore given by

$$\eta_{jm}^{\ 2} = \sum_{k=1}^{K}\sum_{p=1}^{L} r_{jm,kp}^{\ 2} X_{kp,jm}^{\ 2} + \sigma^2 \qquad p \neq m \quad at \ \ k = j$$

Equation 8

The performance improvement due to the ILLRs in a single path, bit- and chip-synchronous environment with uncorrelated fading from bit to bit is huge. The results are demonstrated in Figure 13.

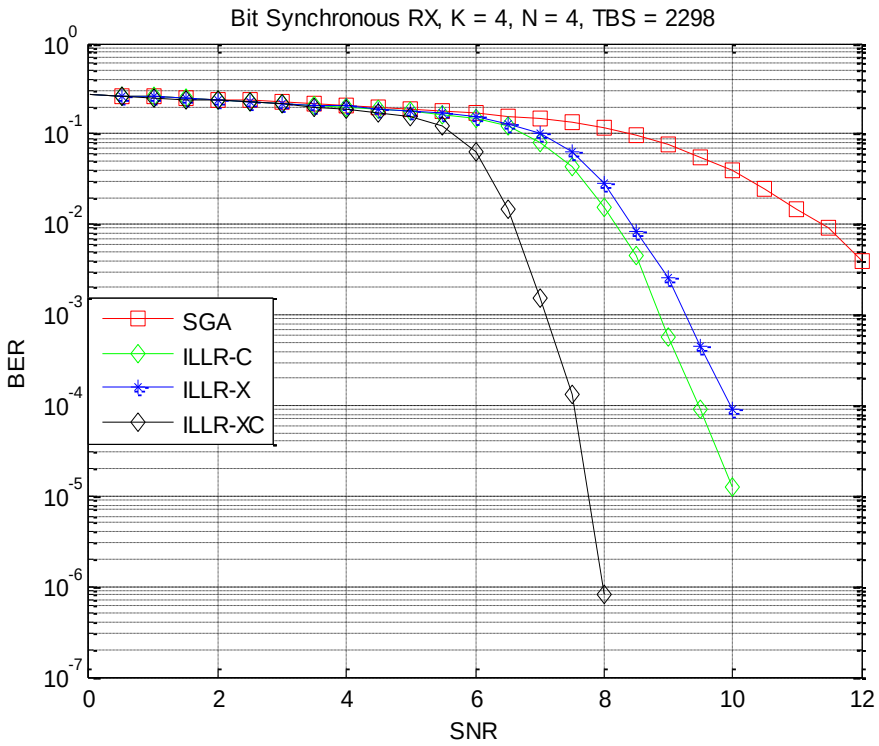

Figure 13: ILLR BER for Bit synchronous reception

The simulation was done with K=4, N=4 and code rate =1/2, TBS = 2298 and Max Log MAP decoder. It is obvious that improved LLRs significantly improve the BER performance for all techniques. The ILLR-X exhibits a gain of excess of about 3 dB as compared to the SGA, and the ILLR-C is slightly better, at a BER of 10^{-2}. At lower BER, the gain is seen to be higher. Finally, the combined knowledge of the channel coefficients and the user cross-correlations resulted in a gain of 6 dB at a BER of 10^{-2}, with higher gains at lower BER.

We quantity the performance gains for more realistic correlated fading channels. To isolate the effect of correlated fading, we simulate bit- and chip-synchronous systems. We chose a small TBS of 2298 with 8 interleaver blocks and high Doppler of 850 Hz in a single path channel.

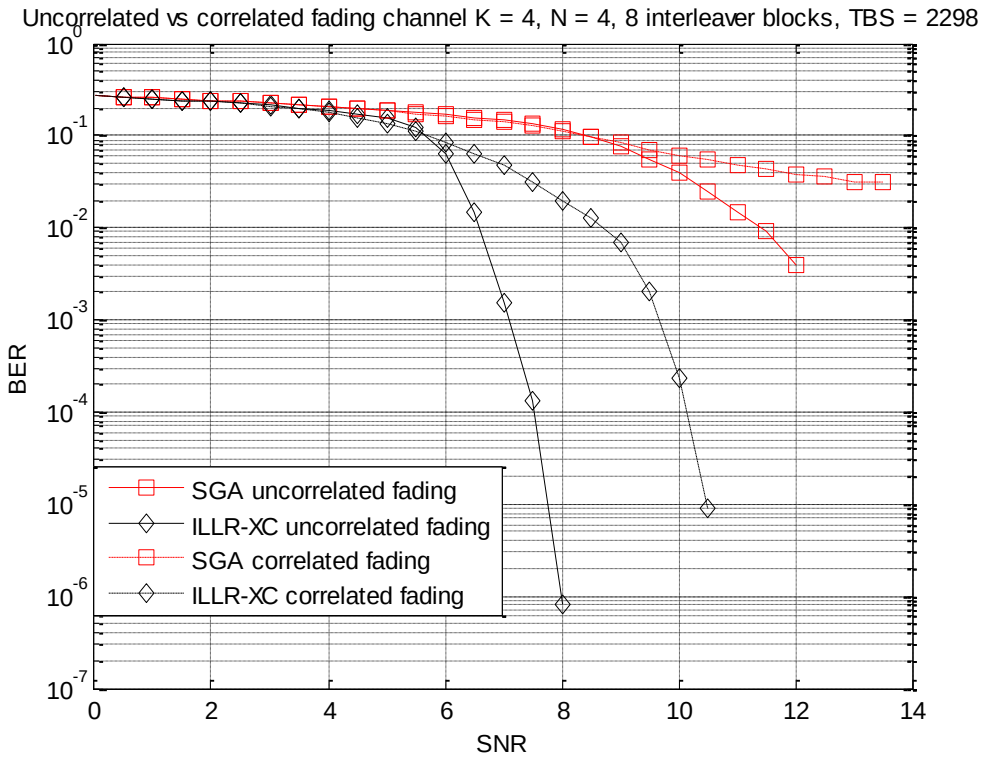

Figure 14: Correlated fading vs. uncorrelated fading for TBS = 2298 and Doppler 850 Hz

The BER for realistic fading channel is around 2.5 dB worse than the uncorrelated fading channel. However, The ILLR-XC is still showing very significant gains. It is also notable that the BER for the SGA saturates in correlated fading channel.

The correlated fading is combated by using large TBS for better interleaving. The TBS of 20730 bits with 8 interleaver blocks is simulated for moderate Doppler (200 Hz) to keep the ratio between interleaver size and Doppler frequency nearly equal.

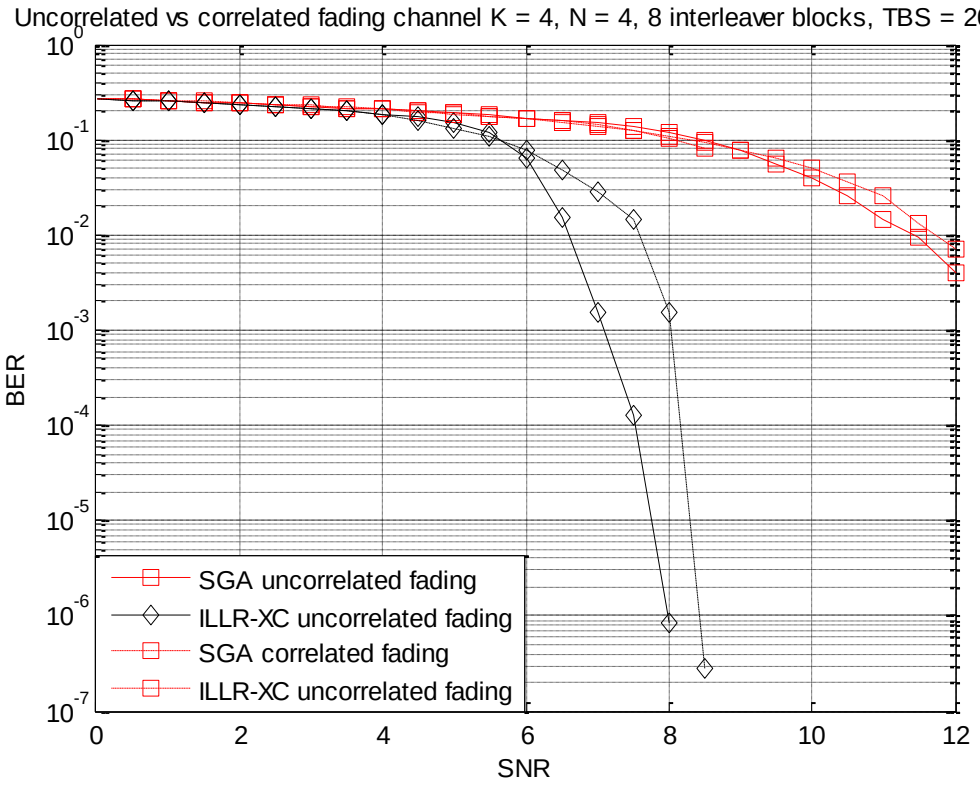

Figure 15: Correlated fading vs. uncorrelated fading for TBS = 20730 and Doppler 200 Hz

It can be seen that the BER performance of the correlated fading channel is worse than the uncorrelated fading by around 0.5 dB. It is also worth noting that the steepness for the correlated fading channel is larger than the uncorrelated fading, this is due to larger TBS block which provides better turbo coder correction capability even for the same coding rate.

Chip Synchronous and Bit Asynchronous Reception

For chip synchronous and bit asynchronous reception, the interference sequence is spread over 2 bits with reference to the user of interest [25]. This is expressed by Advanced 'A' and Delayed 'D' bits of the interfering user.

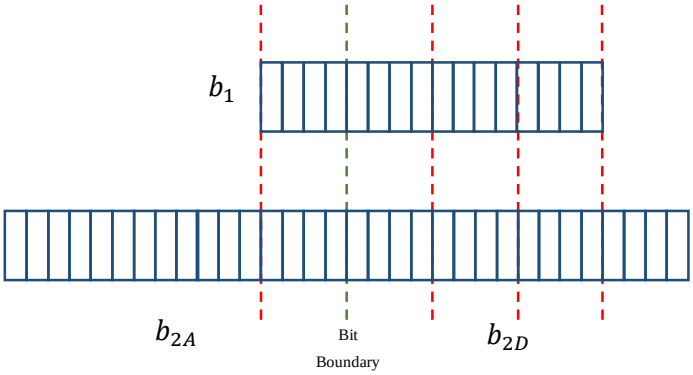

Figure 16: RX of chip synchronous users

The received signal can be expressed as

$$y_1 = b_1 c_{1i} + b_{2\mathrm{A}} c_{2i} + b_{2\mathrm{D}} c_{2i}$$

After passing through the matched filter the output is then sampled at the sampling instants m where $m = 0,1,2,3\,T_c$. The output of the de-spreading operation can be written as

$$y_1 = \left(\left(\sum_{i=0}^{N-1} b_1 c_{1i} \mathrm{E_C} \right) + \left(\sum_{i=0}^{N-1-D} b_{2\mathrm{A}} c_{2i} \mathrm{E_c} \right) + \left(\sum_{i=\mathrm{N}-D}^{N-1} b_{2\mathrm{D}} c_{2i} \mathrm{E_c} \right) \right) * c_{1i}^*$$

where D is the integer chip misalignment factor. E_c is the energy per chip. After that, de-spreading is applied to the previous signal. The previous expression can be written as

$$\mathrm{y_1} = \sum_{i=0}^{N-1} b_1 c_{1i} c_{1i}^* \mathrm{E_C} + \sum_{i=0}^{N-1-D} b_{2\mathrm{A}} c_{2i} c_{1i}^* \mathrm{E_c} + \sum_{i=\mathrm{N}-\mathrm{d}}^{N-1} b_{2\mathrm{D}} c_{2i} c_{1i}^* \mathrm{E_c}$$

$$\mathrm{y_{1d}} = b_1 + b_{2\mathrm{A}} \cdot \frac{1}{\mathrm{N}} \sum_{i=0}^{N-1-D} c_{2i} c_{1i}^* + b_{2\mathrm{D}} \cdot \frac{1}{\mathrm{N}} \sum_{i=\mathrm{N}-D}^{N-1} c_{2i} c_{1i}^*$$

The MAI variance is calculated as

$$\eta_{12}{}^{2} = E\left[\left(b_{2\mathrm{A}}\cdot\frac{1}{\mathrm{N}}\sum_{i=0}^{N-1-D} c_{2i}c_{1i}^{*} + b_{2\mathrm{D}}\cdot\frac{1}{\mathrm{N}}\sum_{i=N-D}^{N-1} c_{2i}c_{1i}^{*}\right)^{2}\right]$$

Equation 9

In [25], it was shown than this expectation can be simplified to

$$\frac{D}{N^2}+\frac{N-D}{N^2}=\frac{1}{N}$$

which is identical to the synchronous case. The instantaneous MAI is calculated as partial cross correlation with the delayed and advanced parts as follows:

$$r_{1j}^{2} = r_{1A}^{2} + r_{1D}^{2}$$

Equation 10

In chip synchronous and bit asynchronous reception, the cross correlations used in Equation 6 and Equation 8 are calculated using partial cross correlations expressed in Equation 10.

The BER performance for bit-asynchronous and chip-synchronous under the same conditions as Figure 13 is shown in Figure 17.

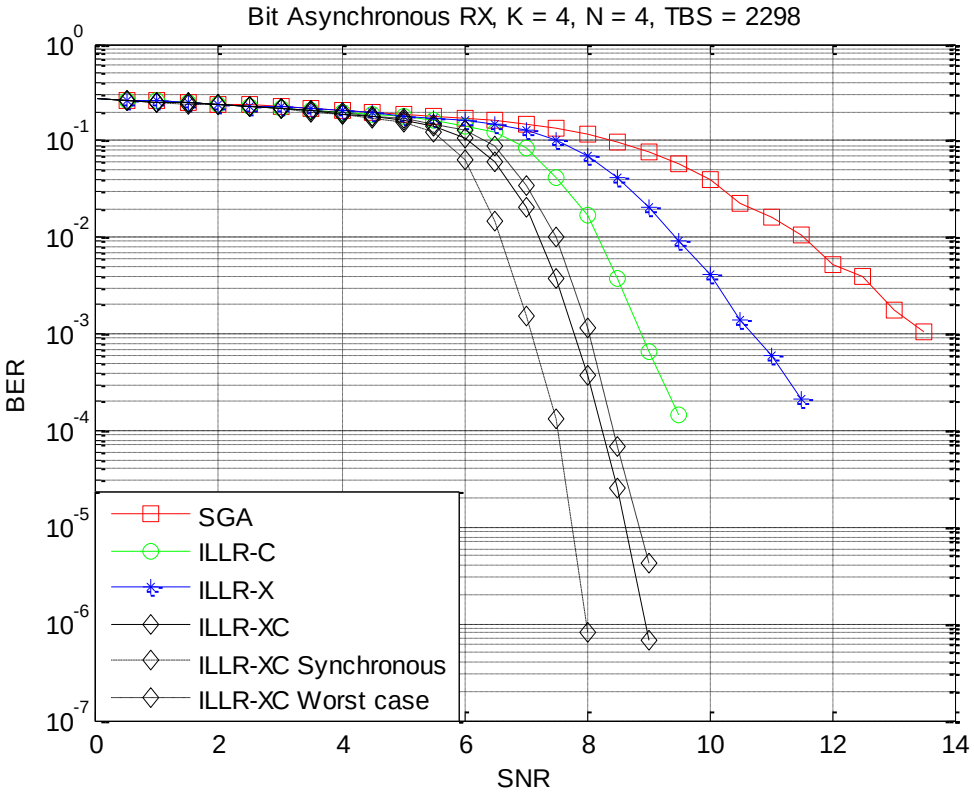

Figure 17: ILLR BER for Chip synchronous reception

The gains are still very evident in the chip synchronous case. It is worth noting that the η^2 in the chip synchronous case is calculated as in Equation 10. There is a worst BER performance when all users are shifted from the user of interest by $T_b/2$, this is depicted in the previous figure with in ILLR-XC worst case. The BER for average user shifts "ILLR-XC" is slightly better than the worse case delay scenario.

CHAPTER 3

3. ASYNCHRONOUS RECEPTION

Chip Asynchronous and Bit Asynchronous Reception

The received signal after despreading in asynchronous multi-path channel can be written as

$$y_{1g} = \sum_{p=1}^{L} |h_{1,l}|^2 \, b_{1,g} + \sum_{p=1}^{L} \sum_{j=2}^{K} |h_{j,p}| \, |h_{1,l}| \cos(\theta_{j,p} - \theta_{1,p}) \sum_{i=g.N}^{g.N+N-1} c_{1,i} \cdot \sum_{n=i-G}^{i+G-\left(\left\lceil \frac{\tau_{j,p}+T_c}{T_c} \right\rceil - 1\right)} b_j, \left\lfloor \frac{n - D_{p,g}}{N} \right\rfloor c_{j,n-D_{p,g}} P\left(\left(i - n - \left\lceil \frac{\tau_{j,p}}{T_c} \right\rceil\right) T_c + \tau_j\right) + n_1$$

Equation 11

where L is the total number of paths. τ_j in this expression resembles the user delays plus the path delay referred to the user of interest.

For chip asynchronous and bit asynchronous reception, each sample from the SRRC/RRC filter of the interfering user is affected by twice the group delay (preceded and succeeded chips), so one or more bits can affect the instantaneous values of the samples. In real systems, the typical spread factor is 64, and the group delay as specified by the standard is six; so it is safe to assume that the single sided group delay is less than the SF. In this analysis, we will consider one interfering user without any loss in generality and later apply the superposition theorem of the independent interfering users.

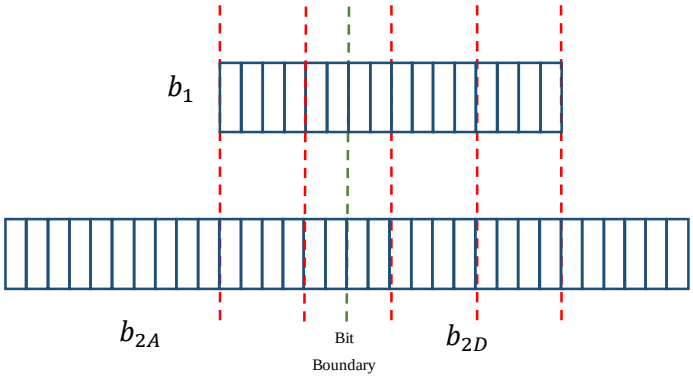

Figure 18: RX of asynchronous users

The MAI at the output of the de-spreading operation for user 2 affecting user 1 can be written as

$$\zeta_{\mathrm{g},12} = \sum_{l=\mathrm{g}N}^{N-1+gN} c_{1l} \left(\sum_{n=l-G}^{l+G-\left(\left\lceil \frac{\tau+T_c}{T_c} \right\rceil - 1\right)} b_{2,\left\lfloor \frac{n-D}{N} \right\rfloor} c_{2,n-D} P\left(\left(\mathrm{l} - \mathrm{n} - \left\lceil \frac{\tau}{T_c} \right\rceil \right) T_c + \tau \right) \right)$$

Equation 12

where D represents the chip misalignment, and τ is the leading time shift as a fraction of T_c that represents fraction of chip misalignment, P respresents the RRC pulse shape, g is the bit index. $\left(\left\lceil \frac{\tau+T_c}{T_c} \right\rceil - 1\right)$ will be donated as α. The previous expression can be generalized for multi-user reception but written in such why to ease the mathematical model. To calculate the MAI variance $\eta_{g,12}^2 = E[\zeta_{g,12}^2]$ so we need to get the expectation over all interfering bits of the $\zeta g_{,12}$ such that we get rid of the bits terms calculate the ILLR.

$$\eta_{\mathrm{g},12}^2 = \mathrm{E}\left[\left(\sum_{l=\mathrm{g}N}^{N-1+gN} c_{1l}\left(\sum_{n=l-G}^{l+G-\left(\left\lceil\frac{\tau+T_c}{T_c}\right\rceil-1\right)} b_{2,\left\lfloor\frac{n-D}{N}\right\rfloor} c_{2,n-D} P\left(\left(\mathrm{l}-\mathrm{n}-\left\lceil\frac{\tau}{T_c}\right\rceil\right)T_c + \tau\right)\right)\right)^2\right]$$

Thus we get.

$$\eta_{g,12}^2 = E\left[\left(\sum_{l=g\mathrm{N}}^{N-1+g\mathrm{N}} c_{1l}\left(\sum_{n=l-G}^{l+G-\alpha} b_{2,\left\lfloor\frac{j-D}{N}\right\rfloor} c_{2,n-N_d} P\left(\left(\mathrm{l}-\mathrm{n}-\left\lceil\frac{\tau}{T_c}\right\rceil\right)T_c + \tau\right)\right)\right).\left(\sum_{m=g\mathrm{N}}^{N-1+\mathrm{gN}} c_{1m}\left(\sum_{k=m-G}^{m+G-\alpha} b_{2,\left\lfloor\frac{k-D}{N}\right\rfloor} c_{2,k-D} P\left(\left(\mathrm{m}-\mathrm{k}-\left\lceil\frac{\tau}{T_c}\right\rceil\right)T_c + \tau\right)\right)\right)\right]$$

Re-ordering the terms yields

$$\eta_{\mathrm{g},12}^2 = E\left[\left(\sum_{l=\mathrm{gN}}^{N-1+g\mathrm{N}}\sum_{n=l-G}^{l+G-\alpha} c_{1l}\, b_{2,\left\lfloor\frac{n-N_d}{N}\right\rfloor} c_{2,n-D} P\left(\left(\mathrm{l}-\mathrm{n}-\left\lceil\frac{\tau}{T_c}\right\rceil\right)T_c + \tau\right)\right).\left(\sum_{m=g\mathrm{N}}^{N-1+g\mathrm{N}}\sum_{k=m-G}^{m+G-\alpha} c_{1m}\, b_{2,\left\lfloor\frac{k-D}{N}\right\rfloor} c_{2,k-D} P\left(\left(\mathrm{m}-\mathrm{k}-\left\lceil\frac{\tau}{T_c}\right\rceil\right)T_c + \tau\right)\right)\right]$$

Doing the expectation over the bits, we get

$$\eta_{g,12}^2 = \left(\sum_{l=\mathrm{gN}}^{N-1+g\mathrm{N}}\sum_{n=l-G}^{l+G-\alpha}\sum_{m=\mathrm{gN}}^{N-1+\mathrm{gN}}\sum_{k=m-G}^{m+G-\alpha} c_{1l}\, c_{1m} c_{2,n-D} c_{2,k-D} P\left(\left(\mathrm{l}-\mathrm{n}-\left\lceil\frac{\tau}{T_c}\right\rceil\right)T_c + \tau\right) P\left(\left(\mathrm{m}-\mathrm{k}-\left\lceil\frac{\tau}{T_c}\right\rceil\right)T_c + \tau\right)\right).E\left[b_{2,\left\lfloor\frac{n-D}{N}\right\rfloor}.b_{2,\left\lfloor\frac{k-D}{N}\right\rfloor}\right]$$

Equation 13

where

$$E\left[b_{2,\lfloor\frac{n-D}{N}\rfloor}.b_{2,\lfloor\frac{k-D}{N}\rfloor}\right]=\begin{cases}1 & \lfloor\frac{n-D}{N}\rfloor=\lfloor\frac{k-D}{N}\rfloor\\ 0 & \text{Otherwise}\end{cases}$$

Equation 14

It is worth noting that the Equation 13 simplifies to the chip synchronous and bit asynchronous case in Equation 9 when $\tau = 0$. It can also be seen that the average value of the MAI depends on the pulse shape characteristics.

Equation 13 can be computed by calculating the conditional variance given the possible bits combinations. For the G<N (easy satisfiable condition), 4 interfering bits need to be included in the MAI variance. The worst case delay "most number of bits needed" at $N/2 < G < N$ occurs at $D = N/2$ with a certain non-zero τ as shown below

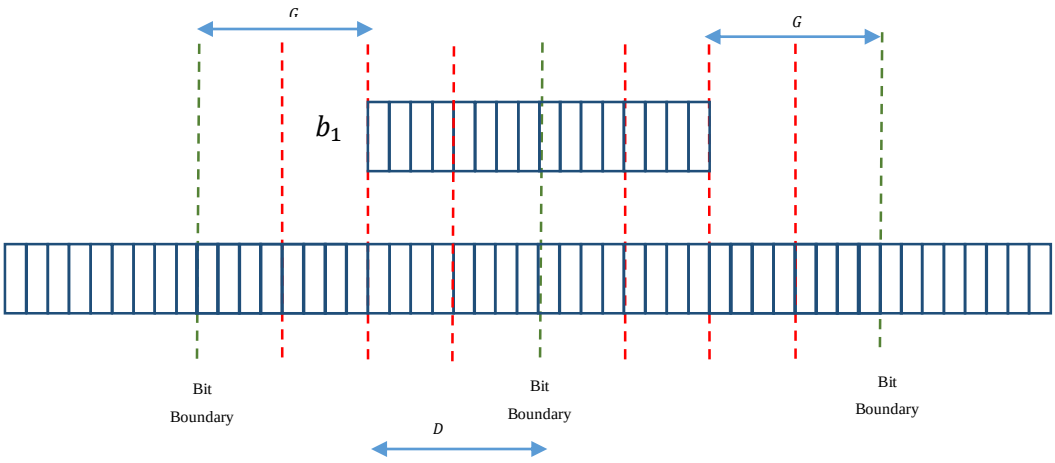

Figure 19: Interfering bits

When $G < N/2$, the worst case delay D, however, occurs when $D = 0$ with a certain non-zero τ as shown below

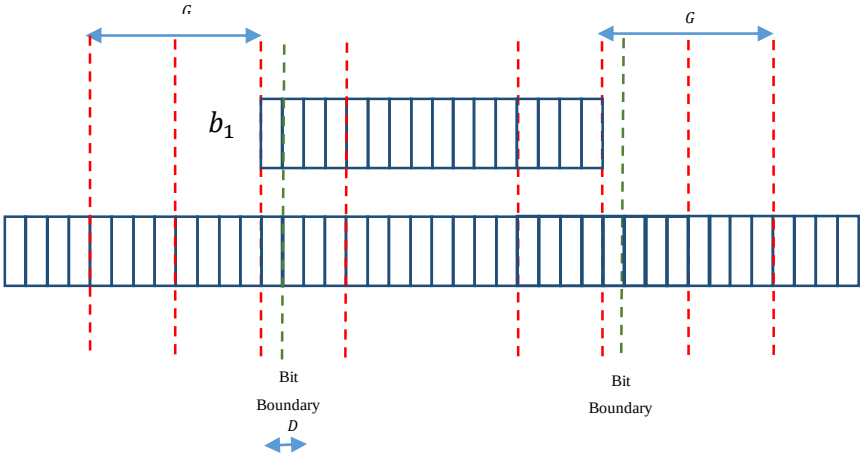

Three bits are needed for calculating the MAI for $G < N/2$.

Those 3 bits form 8 combinations but only four are unique; for example: (+1, +1, -1) is equivalent to (-1, -1, +1). After calculating the conditional MAI variance for all possible combinations, the MAI variance η_{12}^2 can be calculated as

$$\eta_{12}^2 = E[E[\zeta_{12}^2 | b_{n-1}, b_n, b_{n+1}]\,]$$

Equation 15

The number of chips interfering on a single sample can alter the maximum value this sample can take. The number of chips involved in determining the value of a sample is called Truncated Group Delay (G_T). The G_T is thus an approximation of the G considering less number of interfering chips. $G_T < G$ can be used to save the MAI pattern in a lookup table that can speed up the MAI variance calculation. Patterns of MAI conditioned over all possible bit combinations are saved in a computationaly feasible lookup table for fast MAI variance retrieval based on the spreading sequence.

For the special case when $G_T = 1$, Equation 15 will only be affected by 2 bits $(b_{2,A}, b_{2,D})$. $G_T = 1$ is shown later to be a valid assumption for calculating the MAI. In this special case, the MAI signal from user 2 as seen by user 1 can be expressed as

1

$$\zeta_{1g} = \sum_{l=gN}^{D-G-1+gN} c_{1l} \left(\sum_{n=l-G}^{l+G-\alpha} b_{2,A} c_{2,n-D} P\left(\left(l - n - \left\lceil \frac{\tau}{T_c} \right\rceil \right) T_c + \tau \right) \right)$$

$$+\sum_{l=D-G+gN}^{N-1-G-1+gN} c_{1l}\left(\sum_{n=l-G}^{D-1} b_{2,A}c_{2,n-D}P\left(\left(l-n-\left\lceil\frac{\tau}{T_c}\right\rceil\right)T_c+\tau\right)\right. \quad 2$$

$$\left.+\sum_{n=N_d}^{l+G-\alpha} b_{2,D}c_{2,n-D}P\left(\left(l-n-\left\lceil\frac{\tau}{T_c}\right\rceil\right)T_c+\tau\right)\right)$$

$$+\sum_{l=N-1-G+gN}^{D-1+gN} c_{1l}\left(\sum_{n=l-G}^{l+G-\alpha} b_{2,D}c_{2,n-D}P\left(\left(l-n-\left\lceil\frac{\tau}{T_c}\right\rceil\right)T_c+\tau\right)\right) \quad 3$$

where 1 represents when the chip of user 1 is totally affected by b_{2A} only. 2 represents when the chip of user 1 is affected by b_{2A} and b_{2D}. Finally, 3 represents the chips of user 1 are affected only by b_{2D}. The above equations can be written as

$$y_{1g}=b_{2,A}\left(\sum_{l=gN}^{D-G-1+gN} c_{1l}\left(\sum_{n=l-G}^{l+G-\alpha} c_{2,n-D}P\left(\left(l-n-\left\lceil\frac{\tau}{T_c}\right\rceil\right)T_c+\tau\right)\right)\right)$$

$$+b_{2,A}\left(\sum_{l=D-G+gN}^{N-1-G-1+gN} c_{1l}\left(\sum_{n=l-G}^{N_d-1} c_{2,n-D}P\left(\left(l-n-\left\lceil\frac{\tau}{T_c}\right\rceil\right)T_c+\tau\right)\right)\right) \quad 4$$

$$+b_{2,D}\left(\sum_{l=D-G+gN}^{N-1-G-1+gN} c_{1l}\left(\sum_{n=D}^{l+G-\alpha} c_{2,n-D}P\left(\left(l-n-\left\lceil\frac{\tau}{T_c}\right\rceil\right)T_c+\tau\right)\right)\right)$$

$$+b_{2,D}\left(\sum_{l=N-1-G+gN}^{D-1+gN} c_{1l}\left(\sum_{n=l-G}^{l+G-\alpha} c_{2,n-D}P\left(\left(l-n-\left\lceil\frac{\tau}{T_c}\right\rceil\right)T_c+\tau\right)\right)\right) \quad 5$$

$$\eta_{12}^2$$

$$=E\left[\frac{\left[4|b_{2,A}=+1\right]^2+\left[5|b_{2,D}=+1\right]^2+2\left[4|b_{2,A}=+1\right]\left[5|b_{2,D}=+1\right]+\left[4|b_{2,A}=+1\right]^2+\left[5|b_{2,D}=-1\right]^2+2\left[4|b_{2,A}=+1\right]\left[5|b_{2,D}=-1\right]}{2}\right]$$

This simplifies to

$$\eta_{12}^2=\left(\sum_{l=gN}^{D-G-1+gN} c_{1l}\left(\sum_{n=l-G}^{l+G-\alpha} c_{2n-D}P\left(\left(l-n-\left\lceil\frac{\tau}{T_c}\right\rceil\right)T_c+\tau\right)\right)\right)^2$$

$$+\left(\sum_{l=D-G+gN}^{N-1-G-1+gN} c_{1l}\left(\sum_{n=l-G}^{D-1} c_{2,n-D}P\left(\left(l-n-\left\lceil\frac{\tau}{T_c}\right\rceil\right)T_c+\tau\right)\right)\right)^2$$

$$+2\left(\sum_{l=gN}^{D-G-1+gN} c_{1l}\left(\sum_{n=l-G}^{l+G-\alpha} c_{2,n-D}P\left(\left(l-n-\left\lceil\frac{\tau}{T_c}\right\rceil\right)T_c + \tau\right)\right)\right)\left(\sum_{l=D-G+gN}^{N-1-G-1+gN} c_{1l}\left(\sum_{n=l-G}^{D-1} c_{2,n-D}P\left(\left(l-n-\left\lceil\frac{\tau}{T_c}\right\rceil\right)T_c+\tau\right)\right)\right)$$

$$+\left(\sum_{l=D-G+gN}^{N-1-G-1+gN} c_{1l}\left(\sum_{n=D}^{l+G-\alpha} c_{2,n-D}P\left(\left(l-n-\left\lceil\frac{\tau}{T_c}\right\rceil\right)T_c+\tau\right)\right)\right)^2$$

$$+\left(\sum_{l=N-1-G+gN}^{D-1+gN} c_{1l}\left(\sum_{n=l-G}^{l+G-\alpha} c_{2,n-D}P\left(\left(l-n-\left\lceil\frac{\tau}{T_c}\right\rceil\right)T_c+\tau\right)\right)\right)^2$$

$$+2\left(\sum_{l=D-G+gN}^{N-1-G-1+gN} c_{1l}\left(\sum_{n=D}^{l+G-\alpha} c_{2,n-D}P\left(\left(l-n-\left\lceil\frac{\tau}{T_c}\right\rceil\right)T_c + \tau\right)\right)\right)\left(\sum_{l=N-1-G+gN}^{D-1+gN} c_{1l}\left(\sum_{n=l-G}^{l+G-\alpha} c_{2,n-D}P\left(\left(l-n-\left\lceil\frac{\tau}{T_c}\right\rceil\right)T_c+\tau\right)\right)\right)$$

Equation 16

Equation 16 and Equation 13 yield the same results as it is straightforward to see the equivalence between calculating the MAI variance by taking the expectation over the bits, and taking the expected values of the conditional MAI variance conditioned on the interfering user bits. A worked example for the special case when $N = 2$, and $G = 1$ in the Appendix-1.

It is clear that the MAI and thus the ILLR are affected by the RRC pulse shape properties. An in depth analysis of the pulse shape effect is discussed next.

RC Pulse Shaping

Pulse shaping refers to the shape of a chip being transmitted in the time domain. The classical example of the chip shape is the rectangular pulse. The rectangular pulse has a fixed value during the pulse interval; the pulse does not have any tails outside of the chip period. However, the rectangular pulse shape is not so practical in realistic implementations because it has an infinite bandwidth occupancy.

One of the well-known alternative pulse shapes is the Raised Cosine (RC) pulse. The naming of this pulse shape came from the frequency response of this pulse which is characterized by a cosine function raised above the zero level, hence the term Raised Cosine.

RC pulse shape is characterized by β which is the roll off factor, and the symbol time T. The roll off factor represents the excess bandwidth used by the filter occupied beyond the Nyquist bandwidth $\frac{1}{2T}$. β is bounded between 0 and 1 such that at $\beta = 0$ the RC filter simplifies to a rectangular pulse, and at $\beta = 1$ the filter occupies twice the bandwidth required by Nyquist sampling rate. The effect of performing Raised Cosine (RC) pulse shaping is equivalent to passing the chip sequence through two consecutive Square Root Raised Cosine (RRC) filters as shown in Figure 20. The squared root notion is due to the fact that a RRC has a square root frequency response of an RC filter.

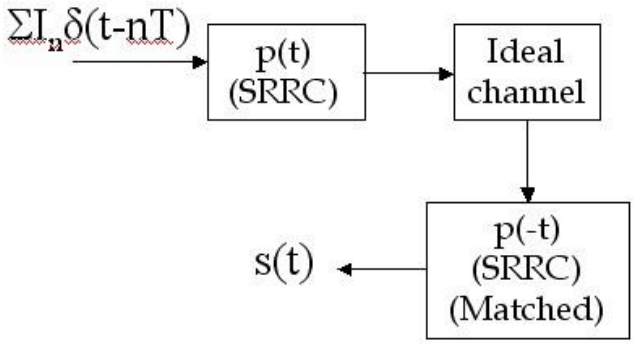

Figure 20: TX & RX RRC in a system [26]

The RC time domain representation is expressed as

$$h(t) = \operatorname{sinc}\left(\frac{t}{T}\right)\frac{\cos\left(\frac{\pi\beta t}{T}\right)}{1-\frac{4\beta^2t^2}{T^2}}$$

Equation 17

The RC time response vary depending on β, an illustration on varying β w.r.t time response is shown below.

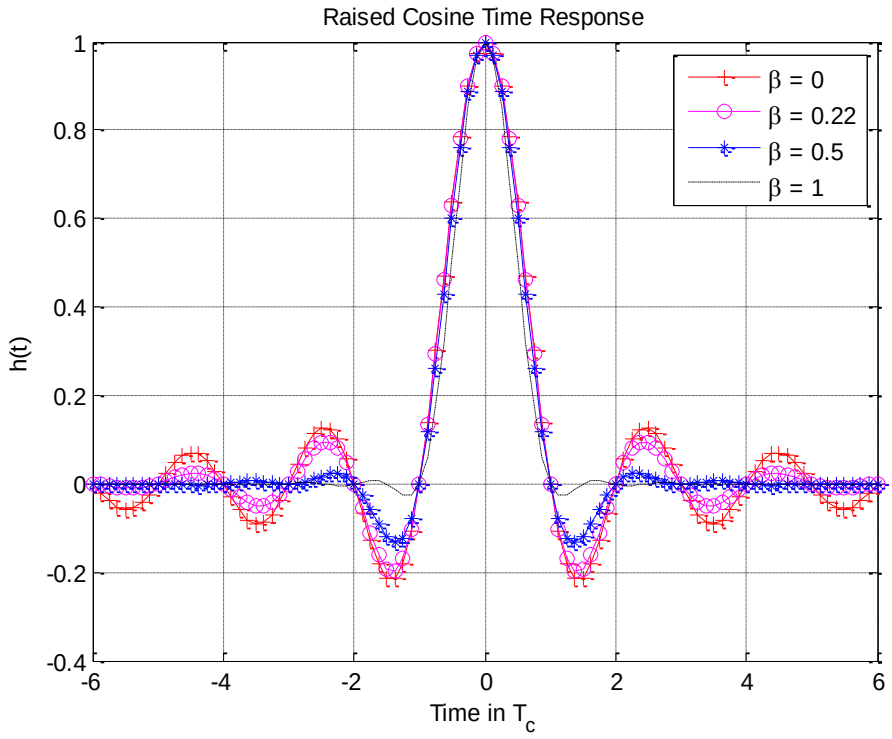

Figure 21: RC Time Response with β a parameter

Increasing β decreases the side lobe level i.e decreases the ISI with the subsequent chips. It is also obvious that the response of one chip is not bounded by the chip time and stretches over other chips "Group Delay" (G). The total response of a chip sequence depends on summation of all these chips at a given instant in time. This phenomena is very important to be noted as it affects our analysis later. It is also noted that the filtered chip has nulls at multiples of T_c to avoid Inter-chip Interference (ICI).

The frequency H_{RC} of the RC filter is expressed in a piecewise notation shown in Equation 18

$$H(f) = \begin{cases} T, & |f| \leq \frac{1-\beta}{2T} \\ \frac{T}{2}\left[1+\cos\left(\frac{\pi T}{\beta}\left[|f|-\frac{1-\beta}{2T}\right]\right)\right], & \frac{1-\beta}{2T} < |f| \leq \frac{1+\beta}{2T} \\ 0, & \text{otherwise} \end{cases}$$

Equation 18

The RC frequency response vary depending on β as well, an illustration on varying β w.r.t frequency response is shown below.

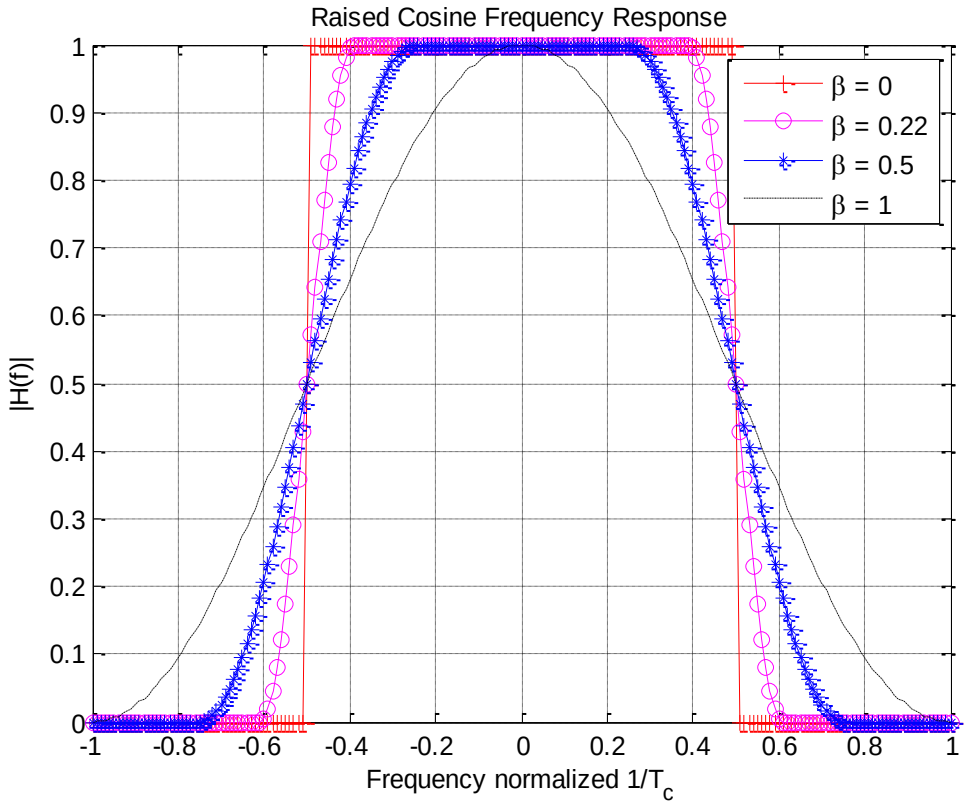

Figure 22: RC Frequency Response vs. β

Increasing β increases the bandwidth occupied by a chip which is not favourable. So, increasing β decreases the side lobe levels (SLL) in the time domain but at the expense of an increase in the bandwidth occupied by the chip in the frequency domain. β=0.22 is chosen by both the CDMA2000 and the 3GPP UMTS standards as the roll off factor with the pulse shape being RRC at the TX and another RRC is used at the RX to get an effect of RC pulse shape.

The RRC time domain representation is expressed as

$$h(t) = \frac{\sin\left(\frac{\pi t}{T}(1-\beta)\right) + \frac{4\beta t}{T}\cos\left(\frac{\pi t}{T}(1+\beta)\right)}{\frac{\pi t}{T}\left(1-\left(\frac{4\beta t}{T}\right)^2\right)}$$

Equation 19

The time response experienced by an RRC filter is similar to that of an RC filter. Increasing β decreases the SLL, however, the peak value of the pulse is a function of β and can exceed 1 in contrast to the RC pulse which has a maximum at the sampling instant with value equal to 1 irrespective of β.

The frequency domain representation of the RRC is expressed as

$$|H_{SRRC}(f)| = \sqrt{|H_{RC}(f)|}$$

Equation 20

where $H_{RC}(f)$ is expressed in Equation 18.

The frequency response is still limited to $-\frac{1}{T} < f < \frac{1}{T}$, similar to that of the RC pulse. The instantaneous amplitudes for time instants other than integer multiple of T_c is affected by the inter-chip Interference (ICI). The ICI can have serious degradation in symbol timing synchronization [27].

The instantaneous interference depends on the relative shift between the user of interest and the interfering users. If the interfering user is aligned with the user of interest, the user of interest will always see an interference of ± 1 (assuming BPSK encoded chips). However, in chip-asynchronous reception, the instantaneous chip interference depends on the interfering user's bit and chip sequence as well as the chip delay of the interfering user relative to the user of interest. Hence, the Probability Density Function (PDF) of the amplitude of a single interfering user signal depends on the relative shift between the user of interest and the interfering user. Figure 23through Figure 27 are the PDF plots of 100 points of the interfering user signal amplitude at relative shifts of $(0, 0.125T_C, 0.25T_C, 0.375T_C,$ and $0.5T_C)$ at $\beta = 0.22$. Due to symmetry, a delay x $> 0.5T_c$ results in a PDF identical to that of 1-x. As expected, the greatest interfering user amplitude spread is at a delay of $0.5T_c$. We also see that a chip misalignment as small as an eighth of a chip results in values that deviate appreciably from {+1,-1}.

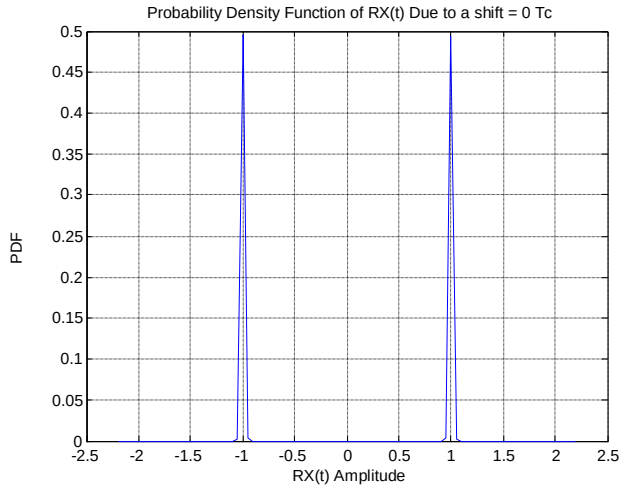

Figure 23: PDF of RX(t) at shift = 0 Tc

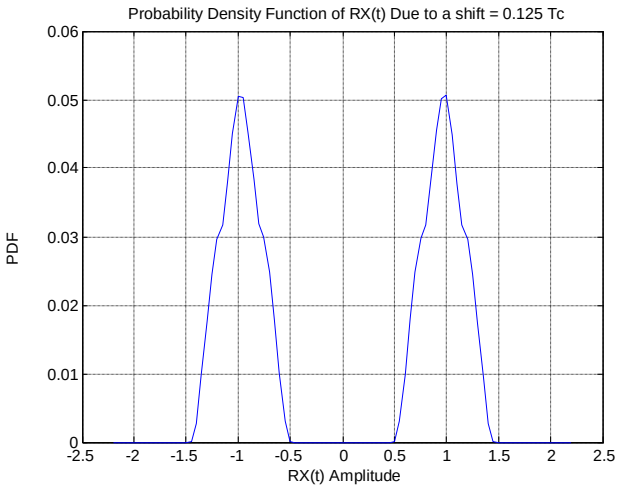

Figure 24: PDF of RX(t) at shift = 0.125 Tc

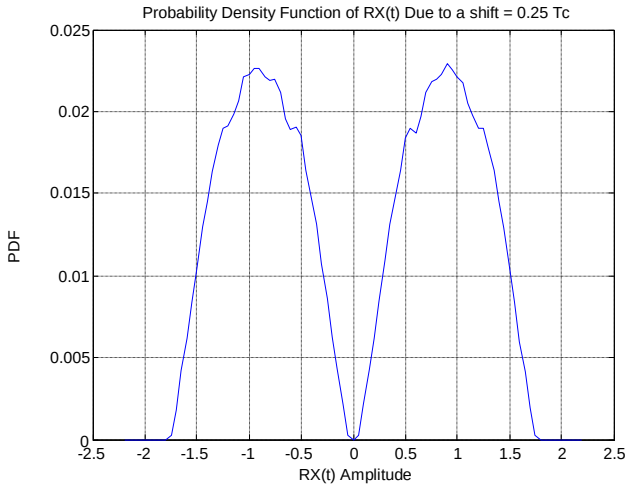

Figure 25: PDF of RX(t) at shift = 0.25 Tc

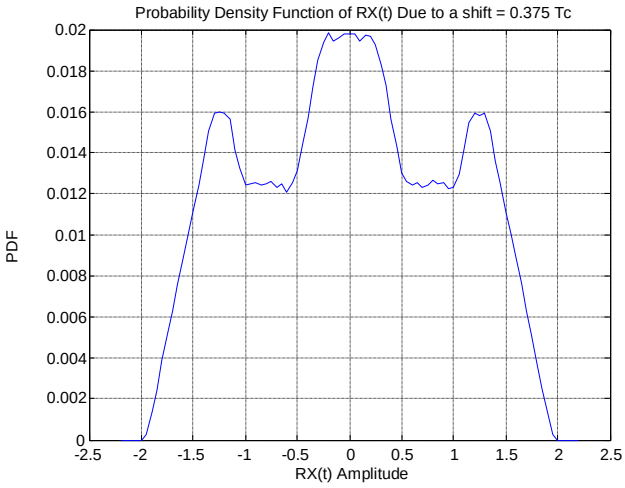

Figure 26: PDF of RX(t) at shift = 0.375 Tc

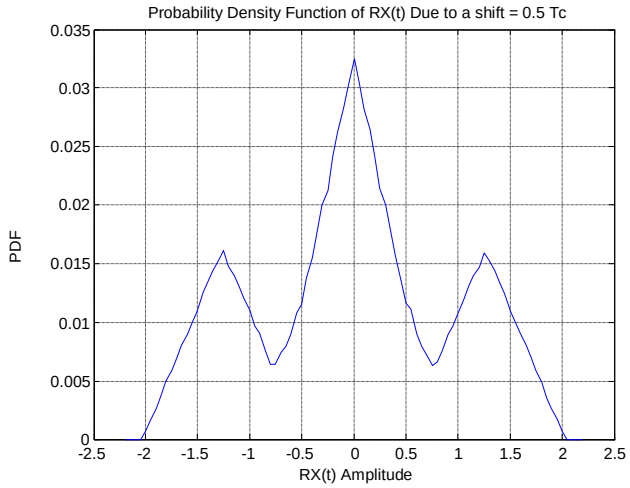

Figure 27: PDF of RX(t) at shift = 0.5 Tc

At shift $= 0$, the interfering users' amplitude are ± 1 with equal probability as illustrated earlier. With a slight shift of $\frac{T_C}{8}$ the distribution spreads both ways around the ± 1. With the shift reaching $\frac{T_C}{4}$. Moving further to shift $\frac{3T_C}{8}$, the PDF is more spread. Reaching shift of $\frac{T_C}{2}$, the PDF now has its maximum spread with maximum interference exceeding ± 2 which is twice the value of the original chips. Due to symmetry considerations further shifts beyond $\frac{T_C}{2}$ is the mirror image of the PDFs around $\frac{T_C}{2}$.

The squared value of the received signal is shown in Figure 29 to Figure 32 with the mean value identified on the plots.

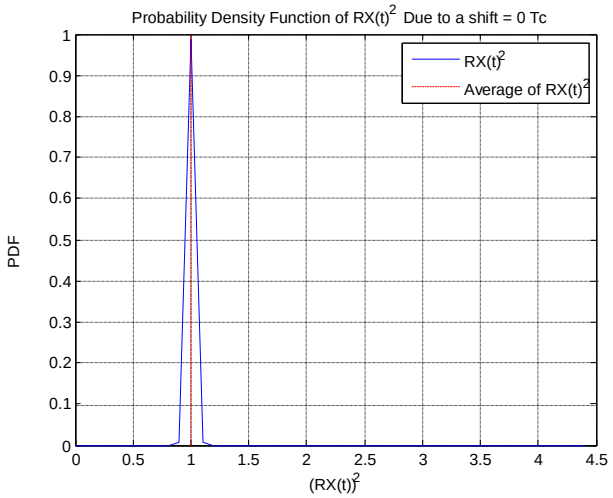

Figure 29: PDF of RX(t)² at shift = 0 Tc

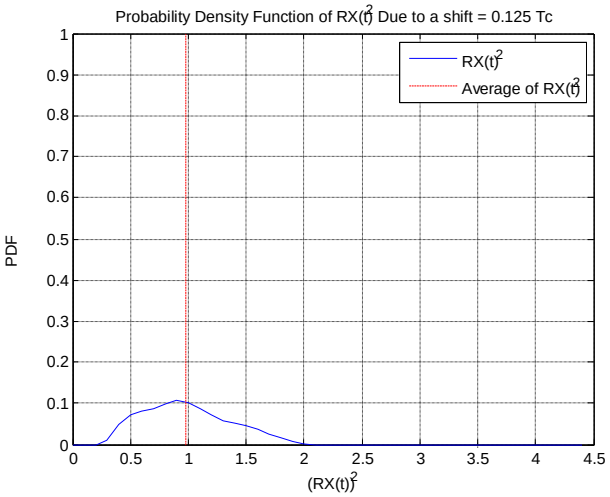

Figure 30: PDF of RX(t)² at shift = 0.125 Tc

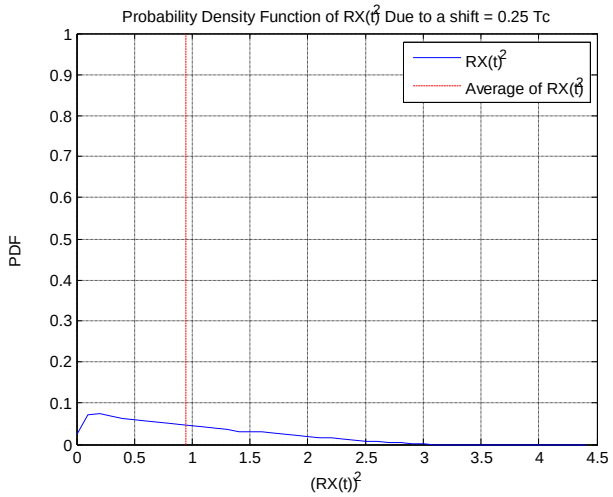

Figure 31: PDF of RX(t)² at shift = 0.25 Tc

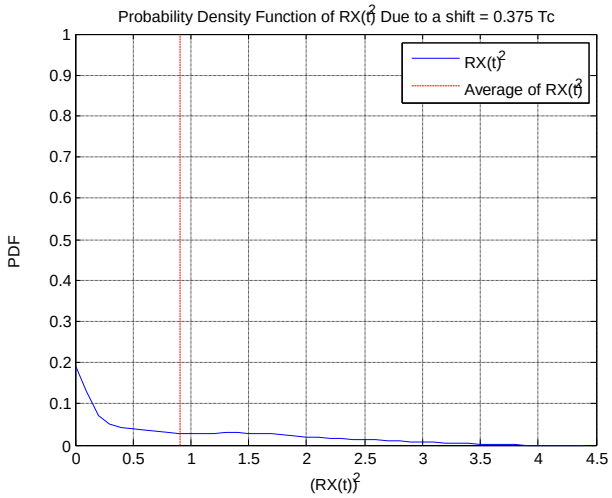

Figure 28: PDF of RX(t)² at shift = 0.375 Tc

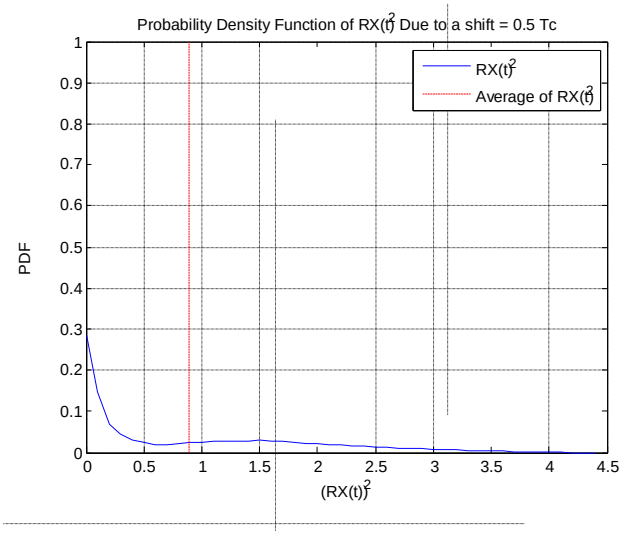

Figure 32: PDF of $RX(t)^2$ at shift = 0.5 Tc

The expected value (mean) of the square of the received signal represents the average power of the interfering user. As expected, the interference power is minimum at $\frac{T_C}{2}$ even though it expresses the maximum amplitude spread shown in Figure 27. This is the smoothing effect of asynchronous transmission on the MAI. For square pulses and averaging over all delays, the variance of MAI is reduced by one third [28]. A theoretical expression of this variance is derived later. Another way of seeing the effect of chip misalignment while varying the roll off factor is to consider the worst-case chip interference, depicted in Figure 33.

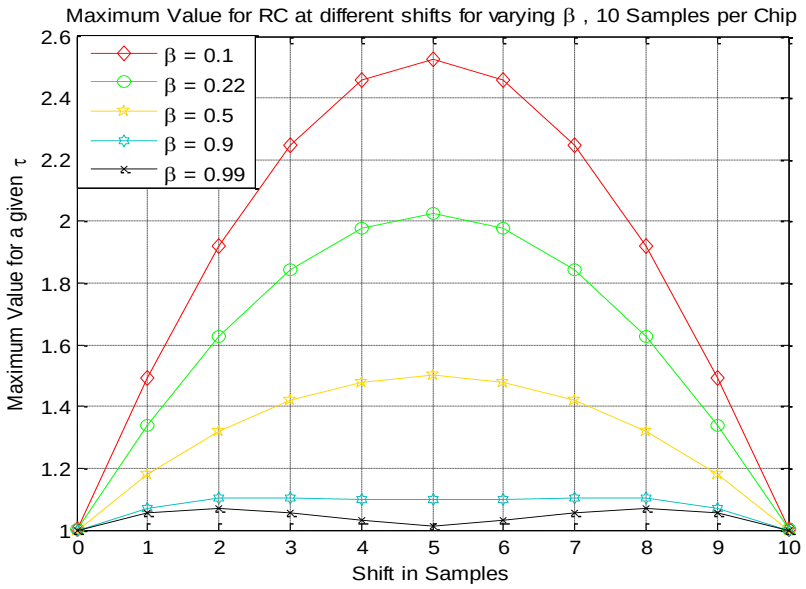

Figure 33: Maximum Value of RC against shift and varyingβ

It can be seen that as the shift increases from 0 to $\frac{T_c}{2}$, the maximum attainable value increases till it reaches a maximum at $\tau = \frac{T_c}{2}$. The effect is mirror-imaged with varying the τ from $\frac{T_C}{2}$ to T_c . As expected, increasing β decreases the maximum value at all given shifts. A group delay of 1000 is used for all roll-off factors. It should be noted that the maximum value a sample can take due to a given shift corresponds to the summation of a worst-case chip sequence, i.e. interfering constructively at this shift.

MAI Variance with RC pulse Shape

In order to model the nature of interference, first we need to get a time domain expression for the interference from a single user. The pulse shape of an interfering user after filtering at the receiver will be equivalent to Raised Cosine (RC) pulse with pulse shape.

$$g(t) = \sqrt{E_c} sinc\left(\frac{t}{T}\right) * \frac{cos\left(\frac{\pi\beta t}{T}\right)}{1 - \left(\frac{2\beta t}{T}\right)^2}$$

Equation 21

The received waveform is expressed as x(t).

$$x(t) = \sum_{k} d_k g(t - kT_c)$$

Equation 22

A sample random waveform of Equation 22 is shown in Figure 34.

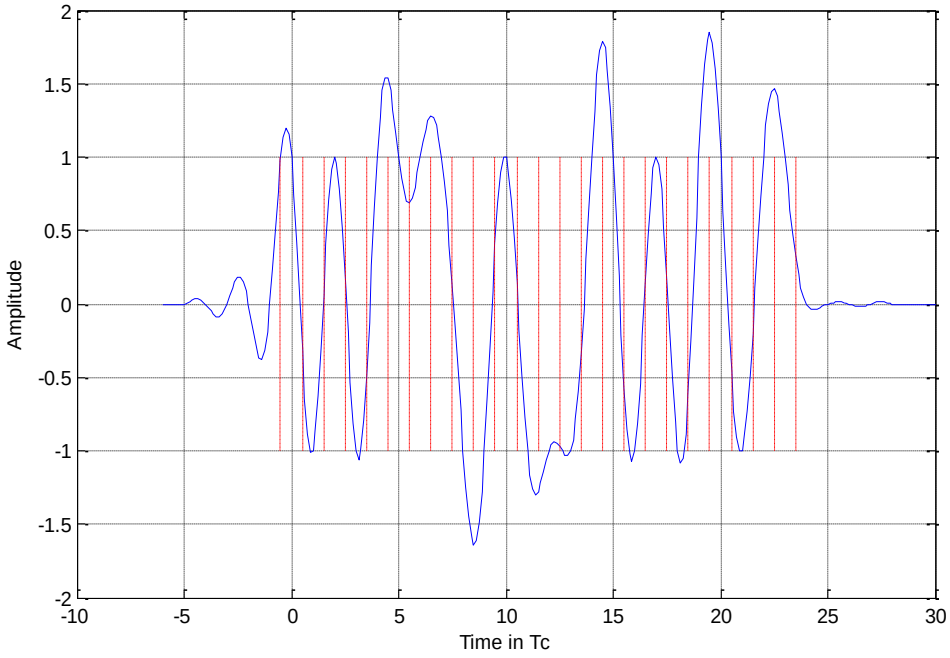

Figure 34: RRC Waveform based on Random Sequence

where d_k is the interfering user chip sequence modulated (i.e. multiplied) by the ± 1 BPSK code bits. The variance of the interfering user can be expressed by

$$var[x(t)] = E\left[\left(\sum_{k} d_k g(t - kT_c)\right)^2\right]$$

Equation 23

This can be expanded to

$$var[x(t)] = E\left[\sum_{k}\sum_{m} d_k g(t - kT_c)\, d_m g(t - mT_c)\right]$$

This is only non-zero when $m = k$, so

$$var[x(t)] = E\left[\sum_{k} g^2(t - kT_c)\right]$$

For pulse shape given in Equation 17, it can be shown that the variance is expressed as follows

$$var[x(t)] = \sum_k E_c \left(sinc\left(\frac{t-k}{T_C}\right).\frac{cos\left(\frac{\pi\beta(t-k)}{T_c}\right)}{1-\left(\frac{2\beta(t-k)}{T_c}\right)^2} \right)^2$$

Equation 24

where E_c is the energy per chip. From this point further, the T_c term will be dropped for convenience and we reinsert it in the final result. A closed form expression for the variance of x(t) is not straight forward in the time domain instead we will do the analysis in the frequency domain equivalence of the above expression using the Fourier transform duality. The $var[x(t)]$ can be expressed using Poisson summation formula [29].

$$var[x(t)] = \sum_k E_c\, g^2(t-kT_c),$$

$$x_v = \int_0^1 \sum_k E_c\, g^2(t-k)e^{-j2\pi vt}dt = \sum_k \int_{k-1}^{k} E_c g^2(t')e^{-j2\pi v(n-t')}\,dt'$$

$$x_v = \int_{-\infty}^{\infty} E_c g^2(t')e^{-j2\pi vt'}dt' = P(-v)$$

where

$$P(v) = G(v) * G(v) = \int_{-\infty}^{\infty} G(u)G(v-u)du$$

Therefore

$$var[x(t)] = \sum_v x_v e^{j2\pi t}$$

$$var[x(t)] = \sum_{v=-\infty}^{v=-\infty} E_c\, G(v) * G(v).e^{-j2\pi vt}$$

Equation 25

$G(v)$ is the Fourier transform of $g(t)$ which is expressed in Equation 17, and $G(v) * G(v)$ represents the convolution of the RC pulse shape with itself. The above expression is summed over v which is an integer value from $-\infty$ to ∞. However, the summation of the convolution outcome is only non-zero at three

values of $v = \pm 1, 0$ with values of $v = \pm 1$ are identical due to the symmetry nature of the pulse shape and the convolution.

$$X_{rc}(f) = \begin{cases} T & 0 \le |f| \le \frac{1-\beta}{2T} \\ \frac{T}{2}\left\{1 + \cos\left[\frac{\pi T}{\beta}\left(|f| - \frac{1-\beta}{2T}\right)\right]\right\} & \frac{1-\beta}{2T} \le |f| \le \frac{1+\beta}{2T} \\ 0 & |f| > \frac{1+\beta}{2T} \end{cases}$$

Equation 26

For $u = 0$

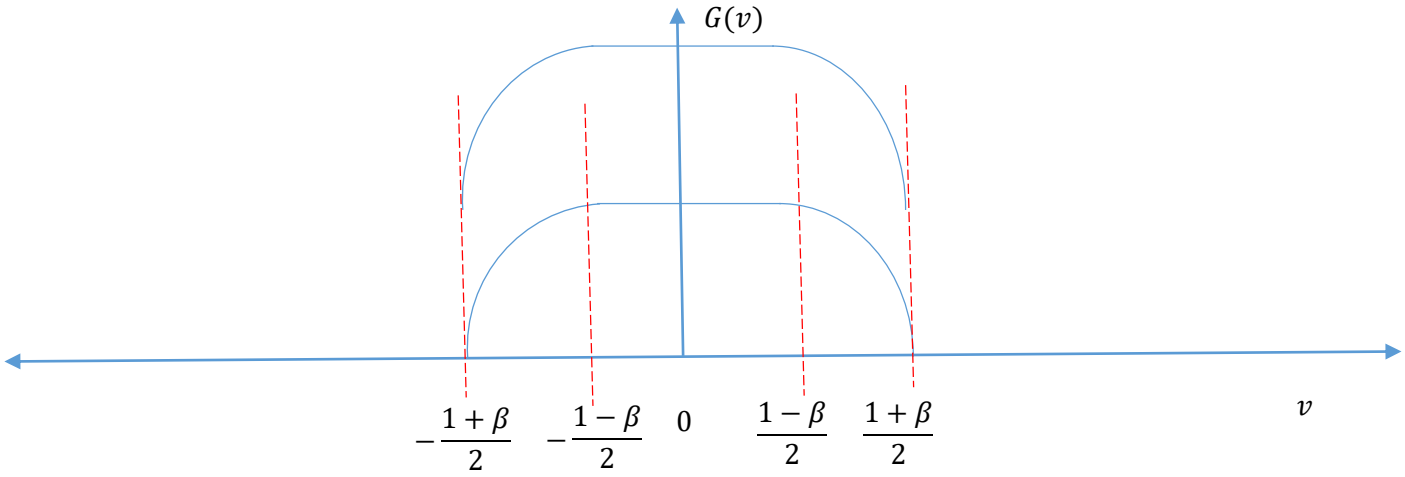

Figure 35: P(0)

$P(0)$ can be expressed as

$$\int_{v=-\infty}^{v=\infty} G(v).G(-v)\,dv$$

$$= \int_{\frac{1-\beta}{2}}^{\frac{1+\beta}{2}} 2\left(\frac{1}{2}\left(1 + \cos\left(\frac{\pi}{\beta}\left(v - \frac{1-\beta}{2}\right)\right)\right)\right).\left(\frac{1}{2}\left(1 + \cos\left(\frac{\pi}{\beta}\left(v - \frac{1-\beta}{2}\right)\right)\right)\right)dv + 2 * \frac{1-\beta}{2} = 1 - \frac{\beta}{4}$$

Equation 27

For $u = 1$

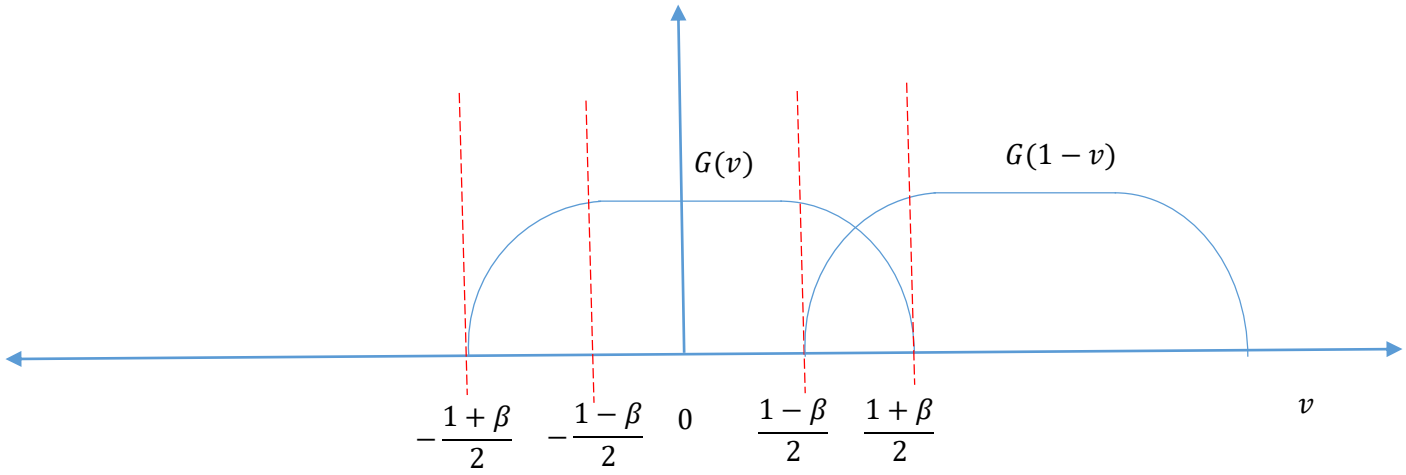

Figure 36: P(1)

$P(1)$ can be expressed as

$$\int_{v=-\infty}^{v=\infty} G(v).G(1-v)\,dv = \int_{0}^{\beta} \left(\frac{1}{2}\left(1+\cos\left(\frac{\pi}{\beta}\left(v-\frac{1-\beta}{2}+\frac{1-\beta}{2}\right)\right)\right)\right). \left(\frac{1}{2}\left(1+\cos\left(\frac{\pi}{\beta}\left(-v-\frac{1-\beta}{2}+\frac{1+\beta}{2}\right)\right)\right)\right) dv = \frac{\beta}{8}$$

Equation 28

Therefore Equation 25 can be simplified to

$$var[x(t)] = E_c\left(\left(1-\frac{\beta}{4}\right)e^{-j2\pi(0)t} + \frac{\beta}{8}e^{-j2\pi(-1)t} + \frac{\beta}{8}e^{-j2\pi(1)t}\right)$$

Equation 29

Finally the $var[x(t)]$ can be expressed as

$$var[x(t)] = E_c T_c\left(\left(1-\frac{\beta}{4}\right) + \frac{\beta}{4}\cos\left(\frac{2\pi t}{T_c}\right)\right)$$

Equation 30

It should be noted that the mean of Equation 30 for different shifts accurately predicts the values plotted through Figure 29 to Figure 32.

Morrow [23] has shown in his work that the MAI after de-spreading for rectangular pulses in an AWGN channel with synchronous and asynchronous reception can be summarized in Table 7.

Table 7: Chip aligned and Chip misaligned MAI for Rectangular pulses [23]

Signal Structure	E[Z]	MAI After De-spreading
Random chip delays, carrier phases aligned	$\frac{2N}{3}$	$\frac{2\,(K-1)}{3\,N}$

where N is the spreading factor, K is the number of users i.e. K-1 is the number of interfering users with respect to the user of interest. Z is the Multiple Access Interference (MAI) variance and E represents the Expected value operator.

Synchronous Reception

Simulating the progressing MAI variance for K = 13 and N=8 across frames can be shown in the figure below. The mean stabilizes to the true mean value after around 300 frames.

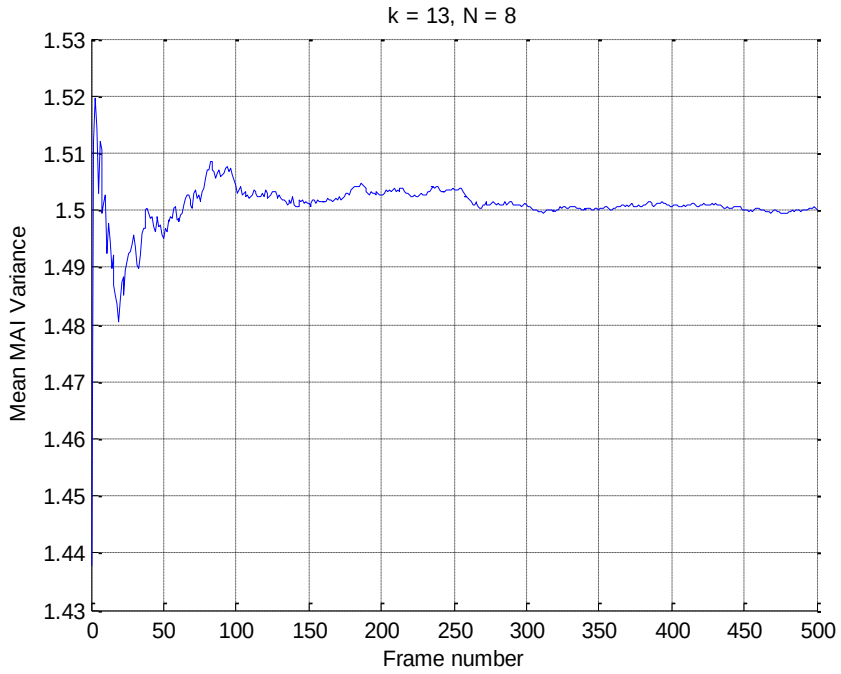

Figure 37: Progressive MAI Variance after De-Spreading for K=13, N = 8

In general the above verification of the expression holds for all values of k and N. The following simulations are run for different k and N at zero noise and BPSK modulation. 500 frames are sent with frame size equal to 1000. Six samples are used per chip, rectangular pulse shape, and random spreading are also used.

Increasing the users from 3 to 7 at N=8 increases the interfering users from 2 to 6 which is 3 folds. This increase linearly maps to increase in the MAI variance as tabulated in the figure above. Further increasing K to 13 doubles the interference from the K =7 case. Doubling the spreading factor effectively reduces the interference to half. The simulated MAI of the previous cases are plotted in the figure below.

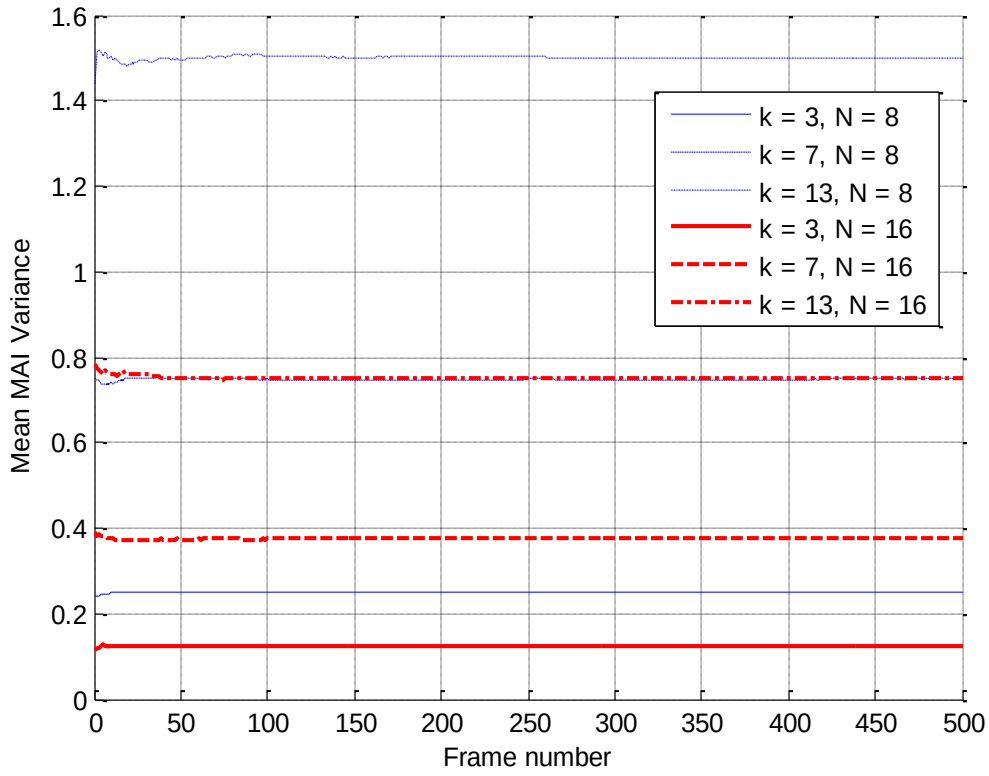

Figure 38: MAI after De-Spreading in chip aligned reception for different K, and N

The simulated steady state mean is exactly as the theoretical expressions assuming no phase offsets.

Asynchronous Reception

For Random chip delays and rectangular pulse shape, the MAI is expressed in Table 7.

Asynchronous reception causes the interference to be smoother, this is clear from the expression that the effective MAI decreases by a factor of 2/3. The respective progressive mean is shown in Figure 39 below.

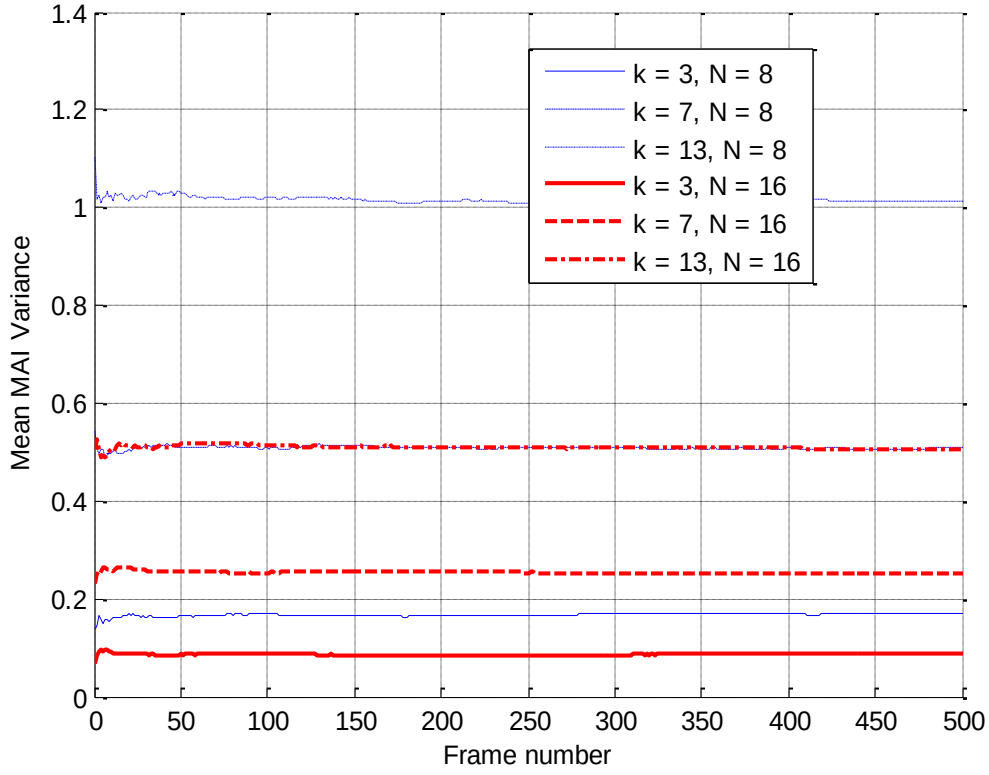

Figure 39: MAI after De-Spreading in chip miss-aligned reception for different K, and N

BER Performance for Synchronous and Asynchronous Reception

The BER can be expressed as

$$P_b = \frac{1}{2}\left(1 - \sqrt{\frac{\gamma}{1+\gamma}}\right), 1/\gamma = \sigma^2 + \frac{K-1}{N}\,\alpha$$

Equation 31

Table 8: Correction term for BER in fading channel

	Chip Synchronous Rect Pulse / RRC	Chip Asynchronous Rect Pulse	Chip Asynchronous RRC
α	1/2	3/2	$(1-\beta/4)/2$

When introducing the fading channel, the BER for synchronous reception is expressed as

$$P_b = \frac{1}{2}\left(1 - \sqrt{\frac{\gamma}{1+\gamma}}\right), 1/\gamma = \sigma^2 + \frac{K-1}{N}$$

Equation 32

while for asynchronous channel in RRC the BER is calculated as

$$P_b = \frac{1}{2}\left(1 - \sqrt{\frac{\gamma}{1+\gamma}}\right), 1/\gamma = \sigma^2 + \frac{1-\frac{\beta}{4}}{2}\frac{K-1}{N}$$

Equation 33

The BER simulation in fading channel is shown below.

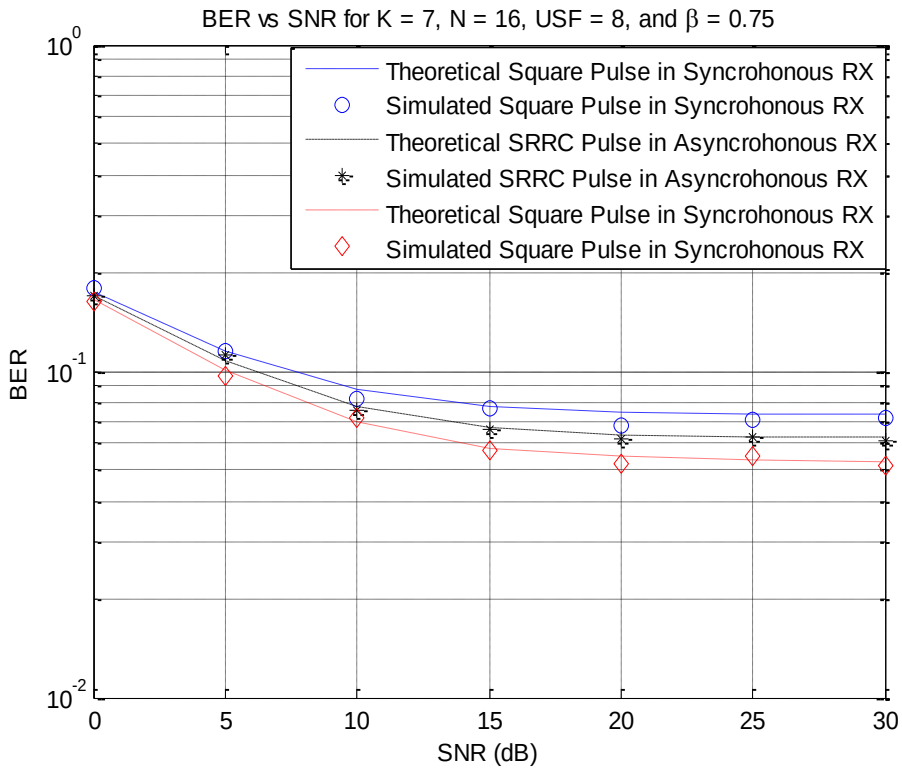

Figure 40: Uncoded BER in fading channel

It should be noted that the theoretical asynchronous expression is derived for square pluses spanning one chip period T_c. It is also worth noting that in synchronous reception, the RRC pulse shape gives identical performance to the square pulse shape; this is due to the fact that in synchronous reception in RRC,

the sampling instants coincide for the user of interest and the interfering users, this causes the interference effect at the matched filter output be exactly as in the square pulse case.

When square root raised cosine pulses are used for transmission and reception, and the users chips are received miss-aligned; the characteristics of the Multiple Access Interference (MAI) change. The instantaneous valued of interference now vary depending on the chip miss-alignment, this creates a variability which is not constant at unity for square pulse shapes. This causes a degradation in BER performance compared to the asynchronous case, yet it is still better than the synchronous reception.

An expression for the MAI variance in the case of the raised cosine pulse at a general miss-alignment delay was derived. It was shown to be

$$var[x(t)] = \left(1 - \frac{\beta}{4}\right) + \frac{\beta}{4}\cos(2\pi t)$$

Equation 34

The interpretation of the previous equation for different roll-off factors is depicted below.

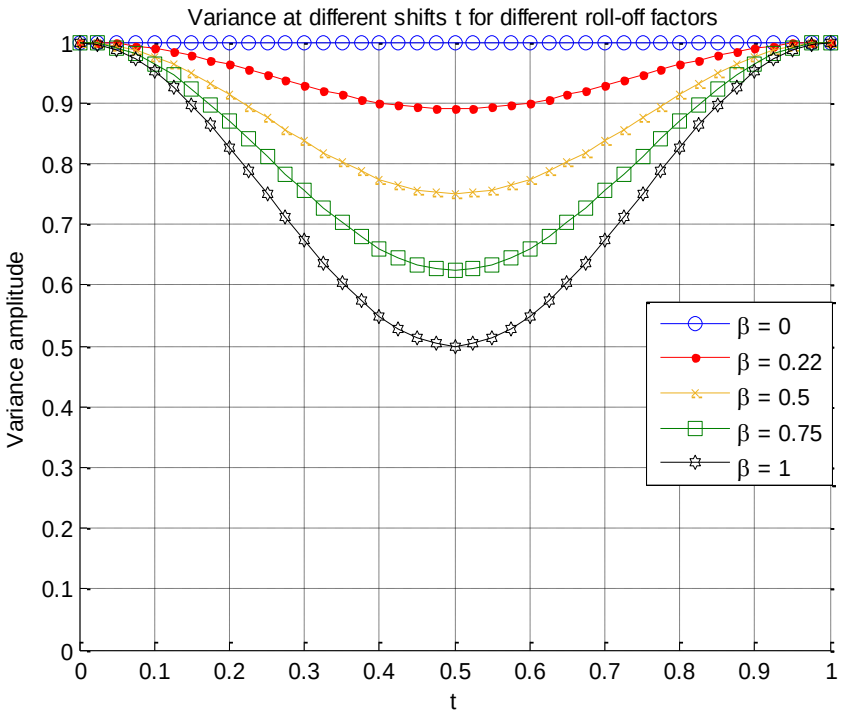

Figure 41: Variance of shifts for different roll-off factors

The previous expression was derived from a sum of squared raised cosine pulse. For the roll off factor $\beta = 0$ "which is the square pulse" it is expected that the sum of raised cosine squared should be constant and equal to unity, this corresponds to the square pulse case. This is confirmed in the figure below for the sum of 501 squared raised cosine pulses terms at group delay $= 200$ and up-sampling factor $= 30$.

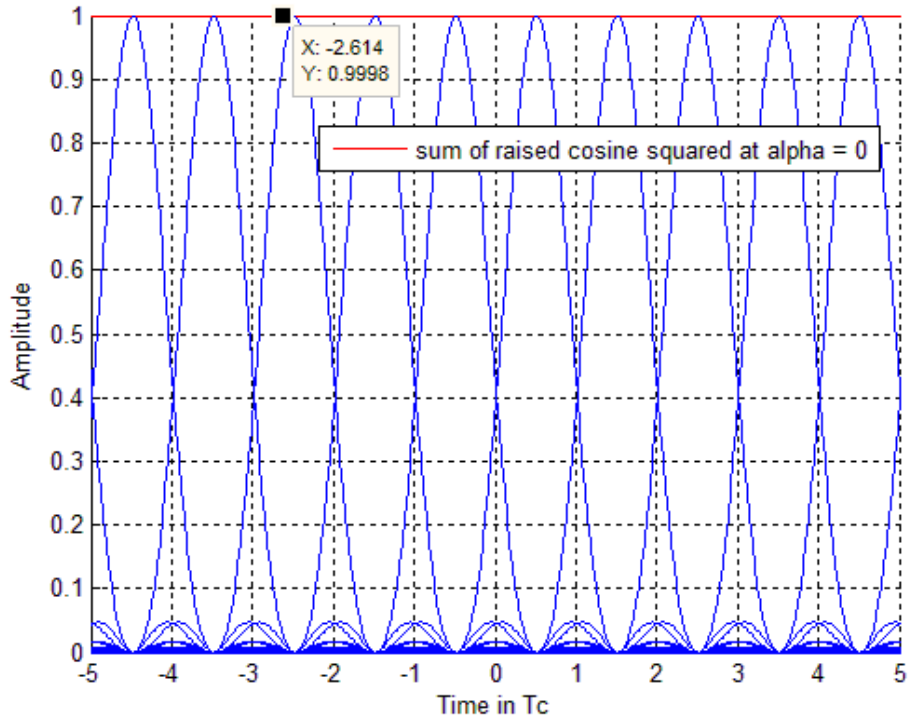

Figure 42: Sum of Raised cosine squared at β=0

For different roll off factors, the variance of $x(t)$ will vary. As expressed below for $\beta = 0.22$ there is a sinusoidal variance across one T_c. The minimum value of variance is at $T_b/2$ and the maximum is at integer multiples of T_c. The maximum value is always equal to unity and the minimum value is equal to

$$\min(var(x(t))) = 1 - \frac{\beta}{2}$$

$$\max(var(x(t))) = 1$$

$$\text{mean}(var(x(t))) = 1 - \frac{\beta}{4}$$

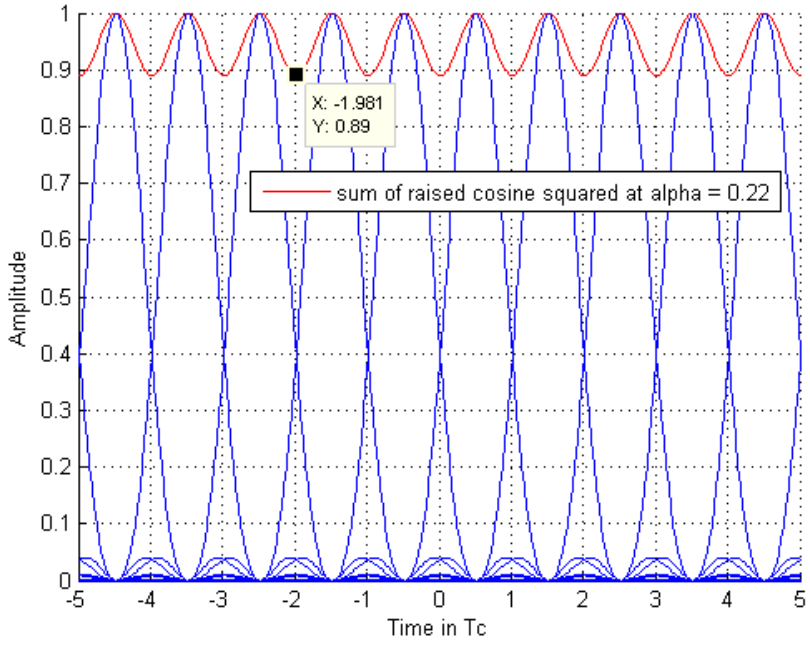

Figure 43: Sum of Raised cosine squared at β=0.22

For $\beta = 1$ and at user shift $= T_c/2$, the variance is equal to 0.5 as shown in the fig below.

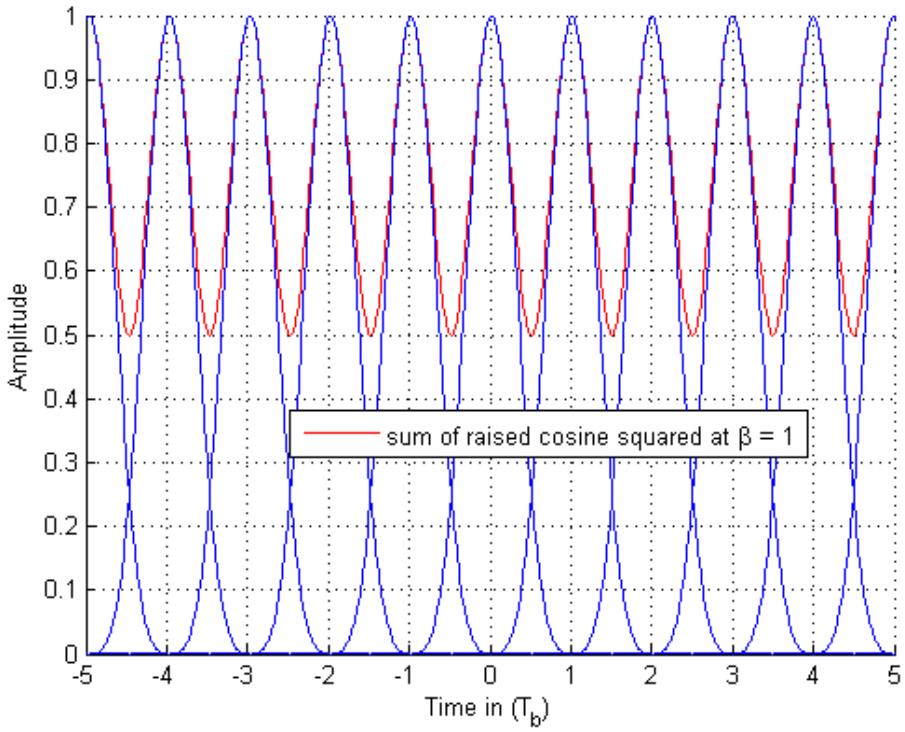

Figure 44: Sum of Raised cosine squared at β=1

CHAPTER 4

4. PERFORMANCE COMPARISON FOR ASYNCHRONOUS MULTI-PATH CHANNELS

A Matlab code was developed to simulate the effect of Improved Log-Likelihood ratios with turbo coding. The Matlab code was optimized to be run on parallel cores to decrease the simulation time.

The simulation parameters of the used system is described next.

Simulation Parameters

The TDD frame structure is shown in [30]. Each frame is 10 ms long consisting of 15 slots; each slot is composed of 2560 chips.

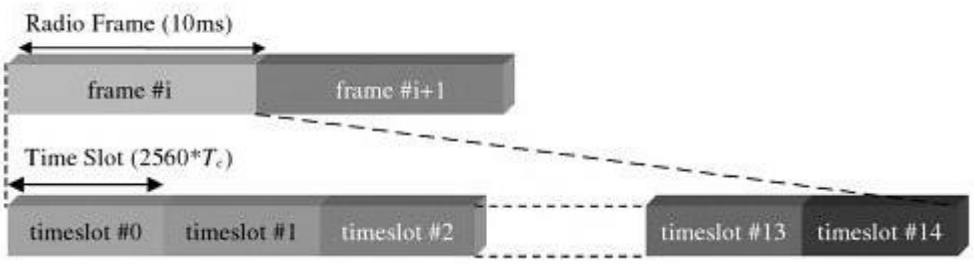

Figure 45: The TDD frame structure

The chip time T_c is calculated as

$$T_c = \frac{10 * 10^{-3}}{15 * 2560}$$

Equation 35

Since each bit is composed of N chips (Spread Factor). So, the bit time T_b is calculated as

$$T_b = \frac{10 * 10^{-3}}{15 * 2560 * N}$$

Equation 36

The code rate (CR) is the reciprocal of the number of code bits per information bit. The Number of samples per code bit N_{sc}

$$N_{sc} = N * USF$$

Equation 37

The Number of samples per bit N_{sb}

$$N_{sb} = N * USF * \frac{1}{CR}$$

Equation 38

The total number of bits in a frame N_b

$$N_b = (TBS + 2 * N_{extra\ bits} + N_{tails\ bits}) * N_{Interleaver\ blocks}$$

Equation 39

The number of samples in a frame N_s

$$N_s = N_b * USF * N$$

Equation 40

Random spreading is used for different users; it has been shown by simulation that the effect of using random spreading is the same as using Pseudo random sequence generator with long sequence.

The CDMA2000 can adapt to wide range of velocities starting from fixed or low mobility handsets to fast speed trains moving at 300 miles/hour [31]. The associated Doppler shift at that speed can be calculated as

$$f_d = \frac{v.f}{c}$$

Equation 41

Where v is the velocity in m/s, f is the operational frequency, and c is the speed of light.

For v = 300 Mile/h, $c = 3 * 10^8$ m/s, $f_c = 1.9$ GHz $\rightarrow$ $f_d \approx 850\ Hz$

The up-sampling factor used is 4 [32] [33]. Where the sampling time $T_s = \frac{Tc}{4}$. The FIR square root raised cosine filter [34] has 48 taps. With the FIR RRC filter being 48 taps and the up-sampling factor used is 4; so the single sided group delay is 6 chips.

For Voice Call the FER can be considered a measurement of the voice quality, since the higher the FER the more distorted the sound is. BLER can be considered a measurement of the radio link quality. It should be less than 2% for voice and less than 10% for PS data calls.

Turbo Decoders

In all mobile networks, there is a need for decoders in the receiver. Whether in the uplink or downlink direction the decoders are essential part of the receiver. The decoders can be hard decoders or soft decoders. In hard decoders, a decision is based on bit bases, while in soft decoders a soft value of the bit is used and a decision is taken after a bulk of bits flow through the decoder. There are different variants of soft decoders such as Soft Output Viterbi Algorithm (SOVA) for turbo codes, and using Maximum Aposteriori Probability (MAP) decoders. The MAP decoders can be further classified as Log MAP, Max* Log MAP, and Max Log MAP decoders. The Max Log MAP decoders are less complex in implementation compared to the Log MAP decoders, but perform about 0.4 dB less than the Log MAP [35]. The Max Log MAP does not rely on the correctness of the input values but instead uses the ratios between the relative probabilities of being a '0' and a '1'. [35] has performed a detailed comparison between the Log MAP and the Max Log MAP decoders and has shown the algorithm to implement them.

The basic equation that determines the soft output decision is the Log Likelihood Ratio (LLR), which is the log of a ratio between the probabilities of being a '1' over being a '0' and is given by

$$LLR_{d_k} = \log \frac{\Pr(d_k = 1 \middle| R_1^N)}{\Pr(d_k = 0 \middle| R_1^N)}$$

Equation 42

The MAP decoding algorithm recursively computes the LLRs of each bit d_k based on a data block N.

Although the calculation of MAP was adjusted for the logarithmic domain to simplify the multiplications involved to additions [36]. The calculation of the logarithm in hardware implementations is not trivial. There are different techniques to calculate the LLRs in practical implementations. The MAP using the logarithm is called Log-MAP calculation and is also referred to as True Log-Map as it is the correct measure of the LLR. The Log-MAP can be closely approximated by max-star (Max*) operator in which

$$\max^*(x, y) = \ln(e^x + e^y)$$

$$= \max(x, y) + \ln\left(1 + e^{-|y-x|}\right)$$

$$= \max(x, y) + f_c(|y - x|)$$

Equation 43

This Max* can be calculated as the maximum of the 2 operands and a correction function f_c If this correction function is set to zero then we reach another approximation called Max-Log MAP. Another approximation (Constant-Log-MAP) uses a constant for the correction function for two entries that are stored as a table. The Linear-Log-Map uses a linear correction to represent f_c. The MAP algorithim and its simplifications are used in turbo decoding. The turbo decoding uses Bahl, Cocke, Jelinek and Raviv (BCJR) algorithm to perform iterative decoding over the transmitted symbols. [37] gives a step by step procedure in calculating the LLRs, and performing the decoding. The Max* and true Log-MAP are sensitive to the correctness of the supplied LLR, while the Max Log-MAP does not change when multiplying by a constant factor.

Channel modelling

Single-Path channel

For a single path Rayleigh fading channel, the bit error probability P_b is given by

$$P_b = \frac{1}{2}\left(1 - \sqrt{\frac{\gamma}{1+\gamma}}\right)$$

Equation 44

Where γ is the effective SNR. In case the energy per bit is equal to unity, γ is given by

$$\gamma = \frac{1}{\frac{N_o}{2} + e\frac{K-1}{N}}$$

Equation 45

$\frac{N_o}{2}$ represents the noise variance, K is the total number of users in the system, N is the spreading factor, and e is a factor representing the

synchronous/asynchronous reception. e is equal to one for synchronous reception.

Multi-Path channel

The presence of multi-path inherently causes diversity, since both paths at the receiver are independent from each other so a deeply faded bit in path i can experience a graceful fading in path j. The rake receiver combines the different paths.

The BER expression in presence of equal-power Multipath is shown in [6] and is expressed as

$$P_b = \left[\tfrac{1}{2}(1-\mu)\right]^L \sum_{k=0}^{L-1} \binom{L-1+k}{k} \left[\tfrac{1}{2}(1+\mu)\right]^k$$

Equation 46

where L is the total number of paths, and μ is expressed as

$$\mu = \sqrt{\frac{\overline{\gamma}_c}{1+\overline{\gamma}_c}}$$

Equation 47

$\overline{\gamma}_c$ is the effective SNR per path and is calculated similar to Equation 45. In Multi-path channels the sum of the absolute of the average channel coefficients should be unity and would represent

Receiver Structure

Rake Receiver

The Rake receiver is a receiver consisting of different fingers. Each finger represents a certain delay of the instantaneous received signal corresponding to a path delay. The Rake receiver then weights each finger with a factor (this weight is the conjugate of the channel coefficient of a given path), then the Rake receiver does Maximum Ratio Combining (MRC) to the fingers. The Rake receiver is used for Multi-path channels. The Rake receiver structure is illustrated in [38].

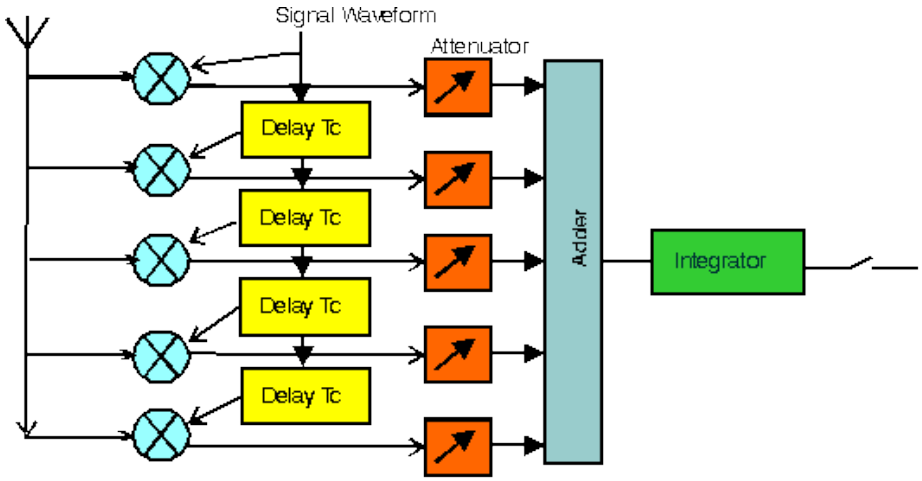

Figure 46: Rake receiver structure

Generalized Rake

The Generalized Rake (GR) is a generalization of the ordinary Rake receiver. It's used to further enhance the BER performance by considering the ICI, Self noise, and breaking the correlations between different paths. The generalized Rake is different from the conventional Rake receiver in 3 major ways

1) The weights of the fingers need not to be the channel taps conjugates
2) The fingers taps can be placed in locations other than and including the channel taps
3) The number of fingers used need not be equal to the number of channel taps (number of paths).

Sundararajan has listed in [39] some GR finger placement algorithms. The number of GR fingers will not lead to significant gains if $J > 2L$ where J is the number of GR fingers and L is the number of multi-path channel tap delays.

[40] has shown that the GR can have a BER advantage over a range between 1.5-2.5dB based on the number of taps used, and the finger placement algorithms.

The GR is a good candidate that may even improve the system performance if implemented.

Simulation Results

Modified SGA based on the pulse shape

In asynchronous reception, we modify the SGA to include the pulse shape effect. The SGA calculation change from Equation 4 to

$$\eta_{jm}{}^2 = \frac{1}{2N}\sum_{p\neq m} E_{jp}(1-\beta/4)/2 + \frac{(K-1)E_b}{2N}(1-\beta/4)/2 + \sigma^2$$

Equation 48

The effect of modifying the SGA is depicted in the figure below. There is a slight gain in including the pulse shape even for the SGA. The SGA before correction performs exactly as the modified expression at low SNR region because the noise variance is the dominant in the MAIN. At high SNR range the effect of introducing the pulse shape is evident.

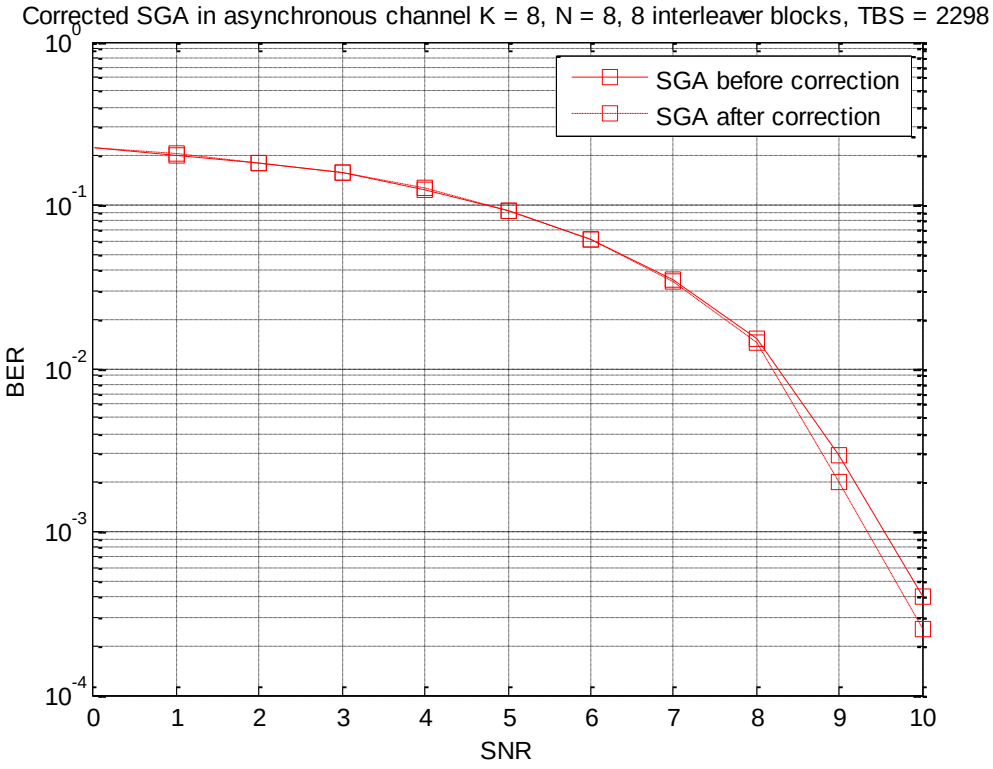

Figure 47: BER after SGA correction for asynchronous reception

The previous simulation is the only simulation done using Max* decoder as the correction term in the Max* decoder is affected by the correctness of the decoder metric as opposed to the Max decoder. The previous simulation was done for 8 users, $N = 8$, 8 interleaver blocks, and TBS = 2298.

Varying Truncated Group Delay

The worst case squared error for various shifts τ is shown in Figure 48.

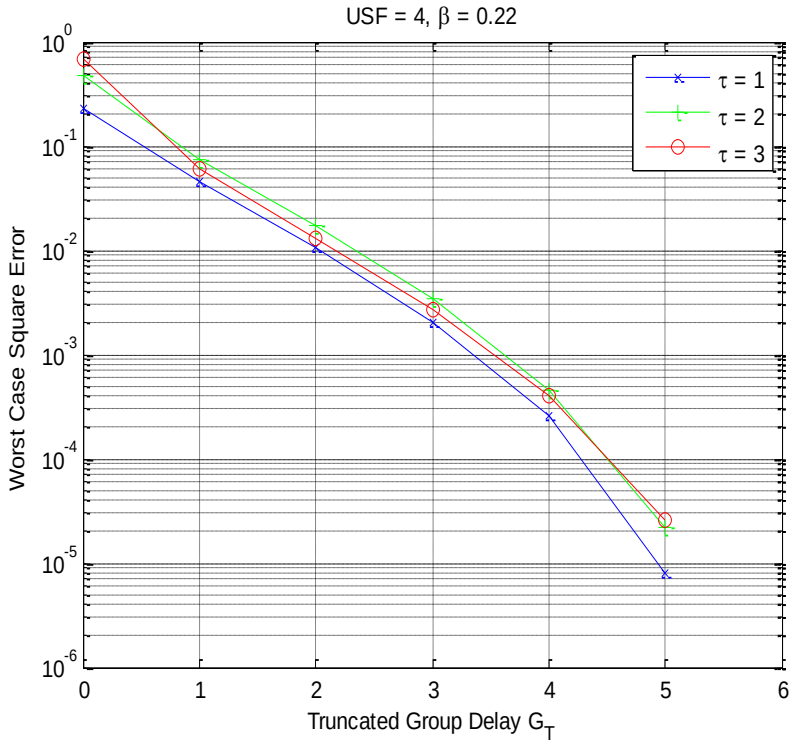

Figure 48: Worst Case Squared error vs. Truncation depth for various shifts

The referencing point to measure the G_T against is using a Group Delay (G) = 6 chips which is the one specified in the CDMA2000 standard. It can be seen that the worst case squared error is less than 10% for all shifts at G_T =1.

The effect of G_T on the BER Performance is shown in Figure 49.

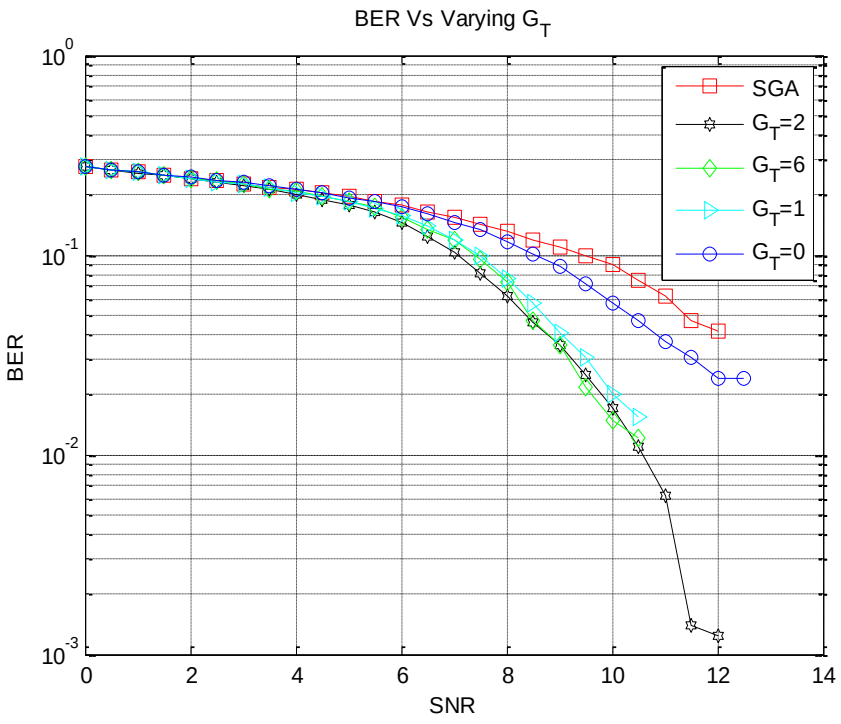

Figure 49: Varying TD on BER performance

The previous figure was done with N=8, K=8, USF=4. The figure shows that even using a G_T of 1, is close enough to using G_T =6 as the worst case squared error was shown to be equal to 10%. Using G_T =0 causes a great loss in BER performance of approximately 2 dB. For G_T = 1 We can see gains of 3dB for ILLR-XC as compared to SGA.

Multi-path

For 2-paths correlated fading channel with the second path delayed from the first path by 26.042 μs and relative power = -3dB in asynchronous reception we can see gains of excess of 2.5 dB as shown below.

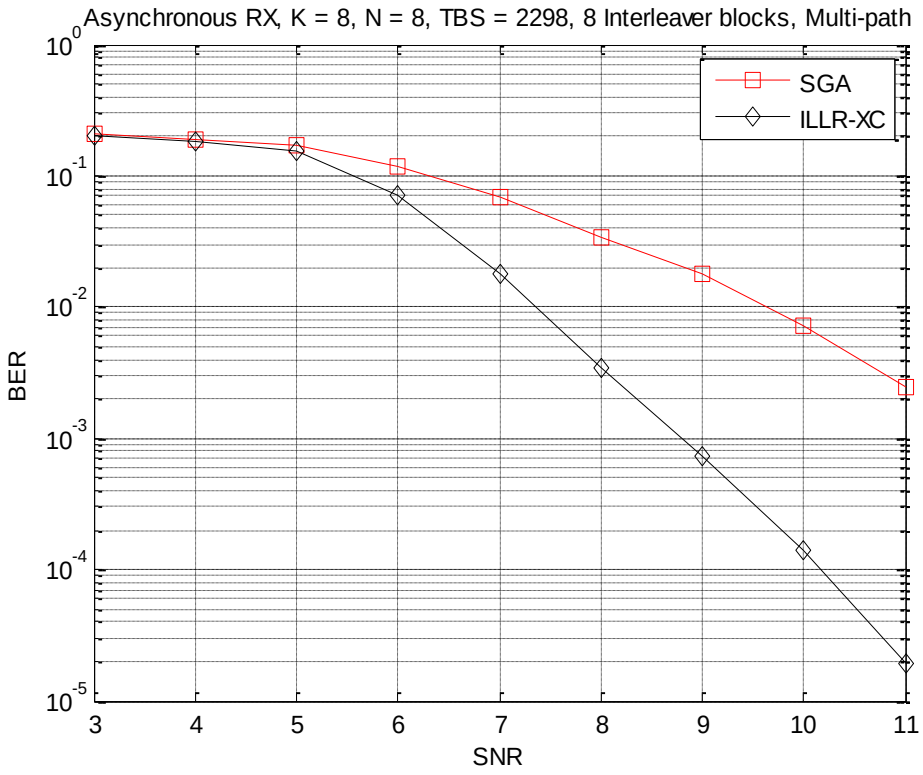

Figure 50: BER for multi-path asynchronous reception

Finally, for more realistic scenario we consider higher spreading factors (N=16) for 4-path correlated fading scenario with coefficients shown in Table 9 [41].

Table 9: 4 Path delays and Path gains

Delay in μs	0	0.11	0.19	0.41
Path Gain in dB	0	-9.7	-19.2	-22.8

The BER for 10 users and $N = 16$ is depicted below.

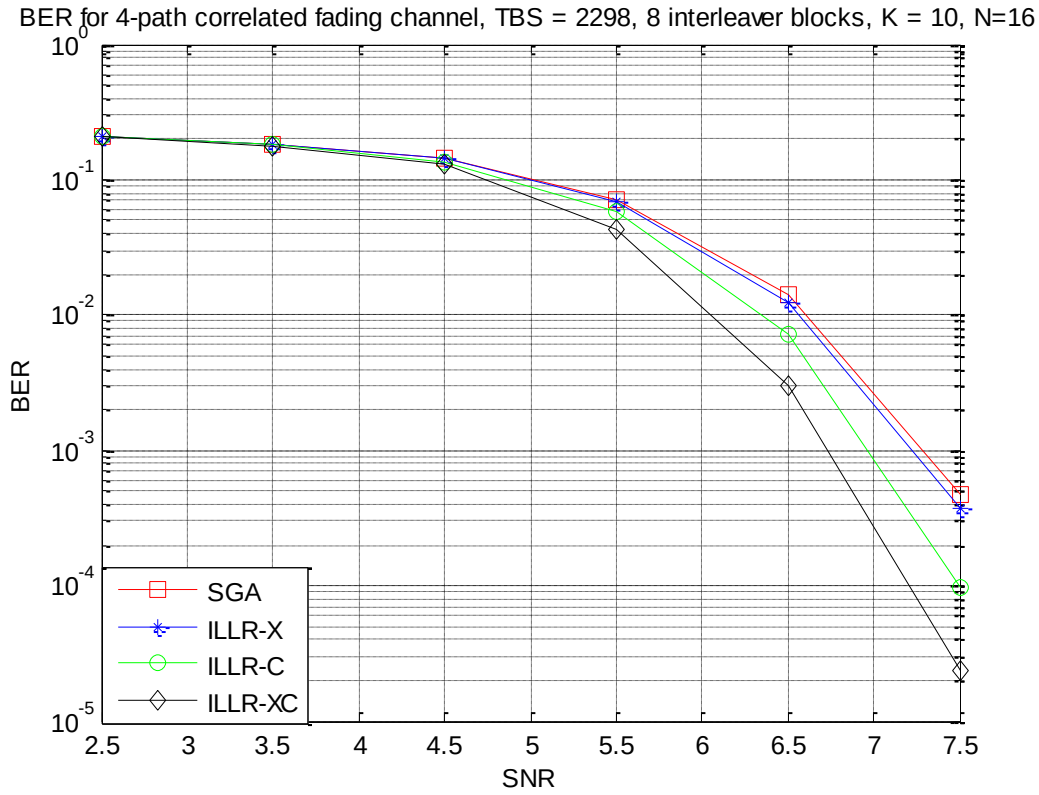

Figure 51: BER for K=10, N=16 in a 4-path correlated fading channel

Since the user loading is moderate, the ILLRs enhance the performance with around 0.75 dB for ILLR-XC. ILLR-C and ILLR-X exhibit lower gains with the channel coefficients being more important that the users cross correlations especially in moderate loading.

The voice communications operate at BLER $= 10^{-2}$. We simulate the block error rate instead of the BER., so the capacity gain due to introducing ILLR-XC is demonstrated by showing the required SNR to achieve this BLER for different loading factors K/N. It is worth noting that the ILLRs exhibit higher gains in BER compared to the BLER. The number of bit errors is counted whether the frame is correct or not so an improvement in decoding is more visible compared to the frame as a unit. In frame errors, a correction in bit errors may or may not result in correct frames so the gains are more visible in BER compared to the BLER. The results are shown below.

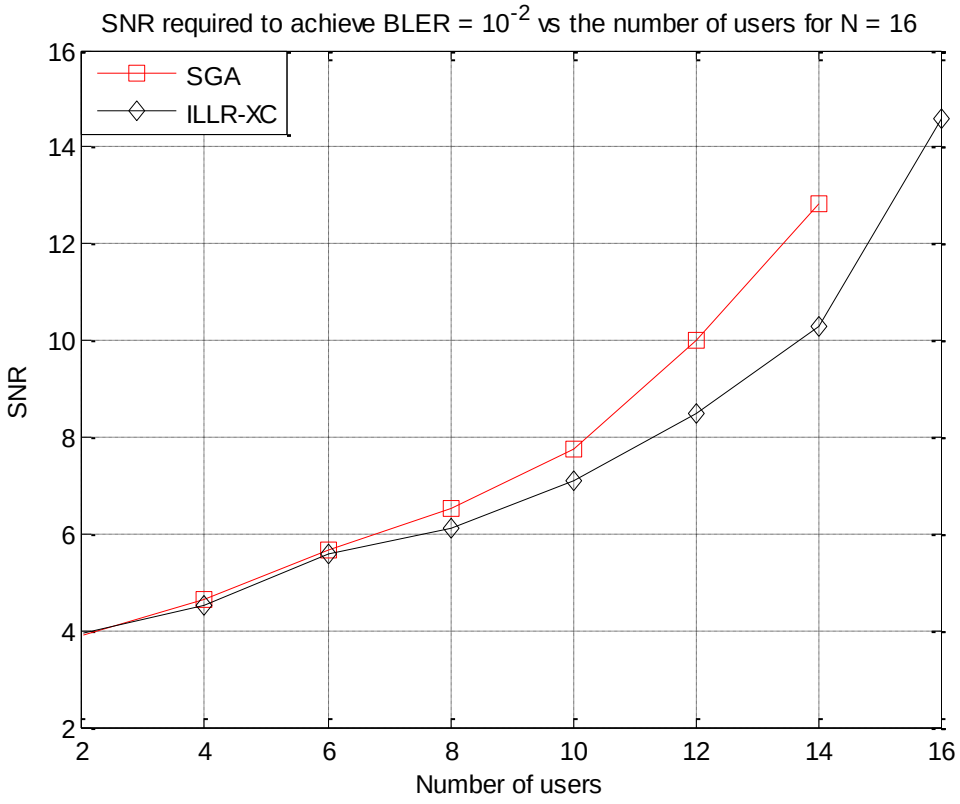

Figure 52: SNR required to achieve BLER = 10^{-2} for various number of users

It can be seen that the ILLR-XC provides larger gains over the SGA when increasing the number of users. A gain of 3dB is achieved for $K/N = 14/16$. For the K/N ratio $= 1$ the performance of the SGA saturates at slightly less than BLER $= 10^{-2}$ in correlated fading channel, so BLER 10^{-2} was not achievable at any SNR. This effect is opposed to Figure 50 in which the second path had relatively larger power than in the realistic scenario which provided better maximum ratio combining and decreasing the saturation effect. The same effect of saturation is evident in the single path correlated fading scenario depicted Figure 14.

Additional simulation results

It is worth showing the effect of changing the coding rate for the same parameters as in Figure 14. The effect of varying the coding rate from 1/2 to 1/3 is shown below.

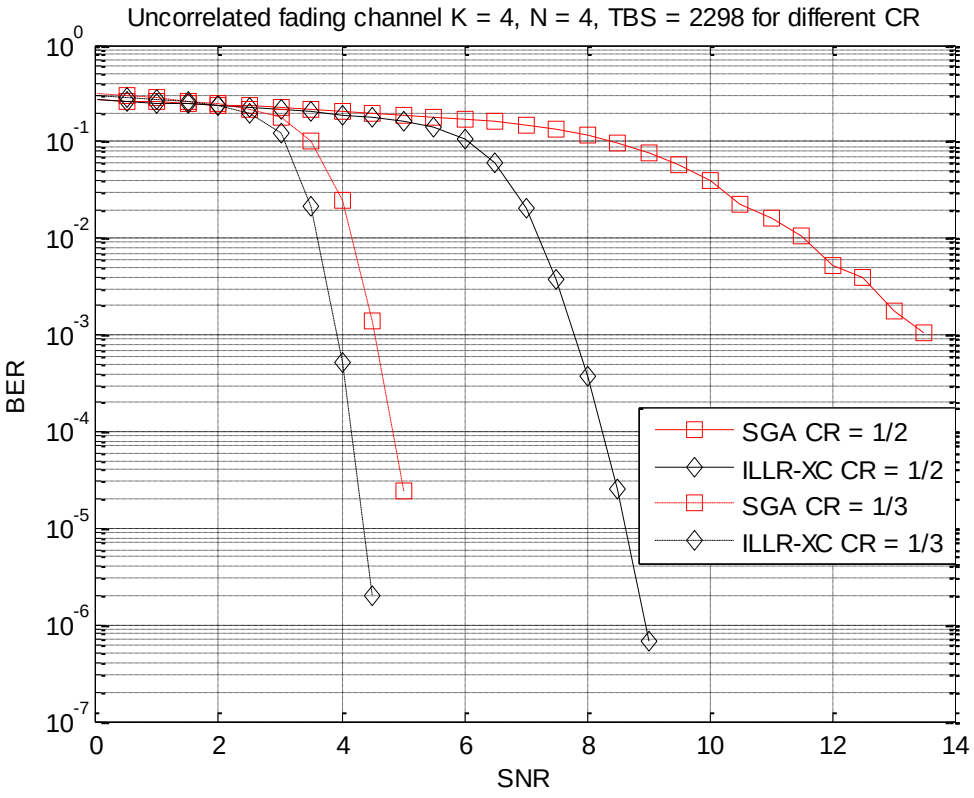

Figure 53: Changing the coding rate effect on ILLR-XC

The BER performance shifted drastically at lower coding rate, also the gains are decreased to less than 1 dB with coding rate 1/3. This is due to the ability of CR 1/3 to correct errors in a better way such that knowing the users cross correlations and channel coefficients does not improve the decoder so much as in the CR = 1/2 does.

CHAPTER 5

5. CONCLUSION

In this thesis, we have presented a novel technique to calculate the LLRs for turbo decoders in 3G systems. ILLR-C, ILLR-X, and ILLR-XC are the proposed techniques to improve the quality of LLRs for the decoders. In synchronous reception, high gains were achieved ranging from 2 to 6 dB. The same gains were observable in bit asynchronous but chip synchronous reception. In Asynchronous reception, a more accurate way to model SGA in the presence of RRC pulse shape was proposed. Also, an expression for conditional variance was derived to be used in ILLR calculation for asynchronous reception. Finally, ILLR-XC can still provide a gain of 3 dB in performance compared to the SGA in multi-path scenarios.

Applying ILLRs to the conventional matched filter detectors is computationally extensive especially in computing the cross-correlations. This thesis did not include the possibility of using ILLRs for interference cancellation, with the metrics being altered to reflect the different statistics of the residual MAI depending on the type of interference canceller. However, the gains from ILLRs alone are significant with the matched filter, resulting in performance comparable to that of some interference cancellers that apply the SGA in the single-user decoders.

Furthermore, the decoder metrics were derived for the matched filter detector under practical conditions. The adoption of specific interference cancellers can be an extension to this work. Another feature of implementing improved decoder metrics is the modularity it affords, where the ILLR may be selectively applied to users suffering higher MAI and/or deep fading. Selectively applying interference cancellation may also be applied in some types of multi-user detectors, e.g. hybrid or group-wise interference cancellers [42], but is more difficult. Finally, the ILLR-X requires the squares, and sums of squares, of cross-correlations. These may be obtained directly without explicit computation of the cross-correlations, and hence more efficiently, as in [43].

Bibliography

[1] "https://ytd2525.wordpress.com/category/lte," [Online].

[2] V. Khairanr, J. Mathur and H. Singh, "Bit Error Rate Performance Analysis of CDMA Rake Receiver," *International Journal of Engineering Science Invention,* vol. 3, no. 6, pp. 52-58, June 2014.

[3] A. Toskala and H. Holma, WCDMA for UMTS : HSPA Evolution and LTE (5th Edition), John Wiley & Sons, Incorporated, 2010.

[4] A. J. Viterbi, CDMA: Principles of Spread Spectrum Communication, vol. 38, MA: Addison-Wesley, 1995.

[5] M. B. Pursley, "Performance Evaluation for Phase-Coded Spread-Spectrum Multiple-Access Communication – Part I: System Analysis," *IEEE Trans. Commun,* vol. 25, no. 8, pp. 795-799, 1977.

[6] J. G. Proakis, Digital Communications, McGraw-Hill, 1995.

[7] S. Verdu, Multiuser Detection, The Press Syndicate of the University of Cambridge, 1998.

[8] M. Juntti and S. Glisic, "Advanced CDMA for Wireless Communications," *Wireless Communications: TDMA Versus CDMA,* vol. 4, pp. 447-490, 1997.

[9] A. Elezabi, "Reliability-based Partial Parallel Interference Cancellation and Iterative Decoding for DS-CDMA over Fading Channels," *ICC,* pp. 4257-4262, 2007.

[10] G. G. Messier and W. A. Krzymien, "Improving channel decoder performance on the CDMA forward link," *Wireless Communications, IEEE Transactions,* 2005.

[11] A. Elezabi and A. Duel-Hallen, "Improved single-user decoder metrics for two-stage detectors in DS-CDMA," *IEEE-VTS Fall VTC ,* vol. 3, pp. pp.1276-1281, 2000.

[12] A. Elezabi and A. Duel-Hallen, "Improved Viterbi decoder metrics for two-stage detectors in DS-CDMA," *Wireless Communications, IEEE Transactions,* Sept 2004.

[13] A. Elezabi, "Improved Turbo Decoding and Interference Cancellation for DS-CDMA with Random Spreading," *VTC Fall,* 2006.

[14] "https://www.qualcomm.com/news/releases/2009/07/05/zte-and-qualcomm-collaborate-boost-umts-system-performance," [Online].

[15] A. Elezabi, "Improved Single-User Decoding with Parallel Interference Cancellation for DS-CDMA over Asynchronous Fading Channels," *WPMC,* 2006.

[16] C. Berrou, A. Glavieux and P. Thitimasjshmia, "NearShannonLimit Error-Correcting Coding and Decoding: Turbo-Codes," *IEEE ICC,* pp. 1064-70, May 1993.

[17] 3GPP, "3GPP TS 36.212 V8.0.0," 2007.

[18] R. S. Martínez, "3G Systems WCDMA (UMTS) & Cdma2000," *Telecommunications Engineering , specializing Telematics,* 2005.

[19] E. A. Yavuz and V. Leung, "A Comparison Study of 3G System Proposals: cdma2000 vs. WCDMA," 2010.

[20] N. Parameshwar and R. Rajagopalan, "A COMPARATIVE STUDY OF CDMA2000 AND W-CDMA," *Award Solutions, Inc,* May 1998.

[21] T. L. Singal, Wireless Communications, Tata McGraw-Hill Education, 2010.

[22] 3GPP, "http://www.3gpp.org/DynaReport/25-series.htm," [Online].

[23] R. K. Morrow, "Accurate CDMA BER Calculations with," *IEEE TRANSACTIONS ON COMMUNICATIONS,,* vol. 46, no. 11, p. 1413, 1998.

[24] D. Divsalar, M. K. Simon and D. Raphaeli, "Improved parallel interference cancellation for CDMA," *Communications, IEEE Transactions,* vol. 46, no. 2, pp. 258-268, 1998.

[25] A. Elezabi, "Improved Single-User Decoding with Parallel Interference Cancellation for DS-CDMA over Asynchronous Fading Channels," *Wireless Personal Multimedia Communications,* 2006.

[26] M. nathan, "gaussianwaves," April 2011. [Online]. Available: http://www.gaussianwaves.com/2011/04/square-root-raised-cosine-filter-matchedsplit-filter-implementation-2/.

[27] L. Seung Joon and N. C. Beaulieu, "Performance of the Raised-Cosine and "Better Than Raised-Cosine" Pulses in Non-Data-Aided Symbol Timing-Error Detection," *Global Telecommunications Conferenc,* pp. 1765-1769, 2007.

[28] M. B. Pursley, "Performance Evaluation for Phase-Coded Spread-Spectrum Multiple-Access Communication--Part I: System Analysis," *Communications, IEEE Transactions,* vol. 25, no. 8, pp. 795-799, 1977.

[29] "http://math.stackexchange.com/questions/1242280/what-is-the-sum-over-a-shifted-sinc-function," [Online].

[30] J. P. Castro, All IP in 3G CDMA Networks: The UMTS Infrastructure and Service Platforms for Future Mobile Systems, John Wiley & Sons, 2005.

[31] Garg, Wireless Network Evolution: 2G to 3G, Pearson Education, 2002.

[32] J. D. Gibson, Mobile Communications Handbook, Third ed., CRC Press, 2012.

[33] 3GPP, "3GPP TS 25.104 V6.8.0," 3GPP, 2004.

[34] E. S. Malki, K. A. Shehata and A. H. Madian, Design of Triple–Mode Digital Down Converter for WCDMA, CDMA2000 and GSM of Software Defined Radio, International Conference Microelectronics (ICM), 2009, pp. 272-275.

[35] H. R. Sadjadpour, "Maximum A Posteriori Decoding Algorithms For Turbo Codes," [Online]. Available: https://users.soe.ucsc.edu/~hamid/PSI00073.pdf.

[36] F. Dowla, Handbook of RF and Wireless Technologies, Newnes, 2003.

[37] S. A. Abrantes, "From BCJR to turbo decoding: MAP algorithms made easier," 2004.

[38] "http://wireless.per.nl/reference/chaptr05/cdma/rake.htm," [Online]. Available: http://wireless.per.nl/reference/chaptr05/cdma/rake.htm.

[39] J. K. Sundararajan, V. Maheshwari and R. D. Koilpillai, "THROUGHPUT ENHANCEMENT IN WCDMA USING THE GENERALIZED RAKE RECEIVER".

[40] G. Kutz and A. Chass, "On the performance of a practical downlink CDMA generalized RAKE receiver," *VTC Fall,* vol. 3, pp. 1352-1356, 2002.

[41] ITU ITU-R M.1225, "Guidelines for evaluations of radio transmission technologies for IMT-2000," 1997.

[42] P. Rathore, V. K. Verma and P. K. Soni, "Hybrid interference canceller enabled spread spectrum receiver," *Computer, Communication and Control (IC4),* 2015.

[43] M. El-Aziz, K. G. Seddik, A. Elezabi and M. Nafie, "Performance and complexity comparison of near-optimal MIMO decoders," *Signals, Systems and Computers, 2013 Asilomar Conference,* 2013.

[44] "LTE-A_Pocket_Dictionary_of_Acronyms," [Online]. Available: http://www.telecomcircle.com/wp-content/uploads/2009/05/LTE-A_Pocket_Dictionary_of_Acronyms.pdf.

[45] 3GPP2, "Physical Layer Standard for cdma2000 Spread," 2004.

1. Worked Example

A worked example for the case of $N = 2$, $N_d = 1$, and asynchronous reception depicted in the figure below

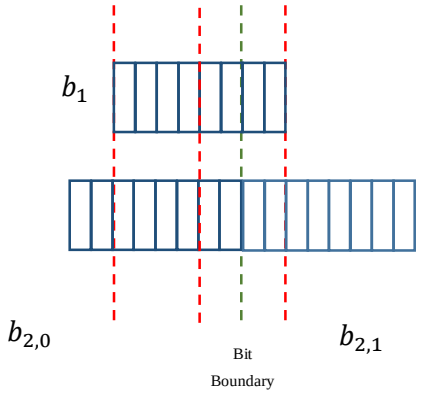

Equation 13 can be expanded to

Index	l	j	m	k		Simplification
1	2	1	2	1	$c_{12}c_{20}c_{12}C_{20}P(\tau)P(\tau)E[b_0b_0]$	$P^2(\tau)$
2	2	1	2	2	$c_{12}c_{20}c_{12}C_{21}P(\tau)P(T_c - \tau)E[b_0b_0]$	$c_{20}c_{21}P(\tau)P(T_c - \tau)$
3	2	1	3	2	$c_{12}c_{20}c_{13}C_{21}P(\tau)P(\tau)E[b_0b_0]$	$c_{12}c_{20}c_{13}C_{21}P^2(\tau)$
4	2	1	3	3	$c_{12}c_{20}c_{13}C_{22}P(\tau)P(T_c - \tau)E[b_0b_1]$	0
5	2	2	2	1	$c_{12}c_{21}c_{12}C_{20}P(T_c - \tau)P(\tau)E[b_0b_0]$	$c_{21}c_{20}P(T_c - \tau)P(\tau)$
6	2	2	2	2	$c_{12}c_{21}c_{12}C_{21}P(T_c - \tau)P(T_c - \tau)E[b_0b_0]$	$P^2(T_c - \tau)$
7	2	2	3	2	$c_{12}c_{21}c_{13}C_{21}P(T_c - \tau)P(\tau)E[b_0b_0]$	$c_{12}c_{13}P(T_c - \tau)P(\tau)$
8	2	2	3	3	$c_{12}c_{21}c_{13}C_{22}P(T_c - \tau)P(T_c - \tau)E[b_0b_1]$	0
9	3	2	2	1	$c_{13}c_{21}c_{12}C_{20}P(\tau)P(\tau)E[b_0b_0]$	$c_{13}c_{21}c_{12}C_{20}P^2(\tau)$
10	3	2	2	2	$c_{13}c_{21}c_{12}C_{21}P(\tau)P(T_c - \tau)E[b_0b_0]$	$c_{13}c_{12}P(\tau)P(T_c - \tau)$
11	3	2	3	2	$c_{13}c_{21}c_{13}C_{21}P(\tau)P(\tau)E[b_0b_0]$	$P^2(\tau)$
12	3	2	3	3	$c_{13}c_{21}c_{13}C_{22}P(\tau)P(T_c - \tau)E[b_0b_1]$	0

13	3	3	2	1	$c_{13}c_{22}c_{12}C_{20}P(T_c - \tau)P(\tau)E[b_1b_0]$	0
14	3	3	2	2	$c_{13}c_{22}c_{12}C_{21}P(T_c - \tau)P(T_c - \tau)E[b_1b_0]$	0
15	3	3	3	2	$c_{13}c_{22}c_{13}C_{21}P(T_c - \tau)P(\tau)E[b_1b_0]$	0
16	3	3	3	3	$c_{13}c_{22}c_{13}C_{22}P(T_c - \tau)P(T_c - \tau)E[b_1b_1]$	$P^2(T_c - \tau)$

η^2 can be calculated by summing the last column of the table such that

$$\eta^2 = 2P^2(\tau) + 2P^2(T_c - \tau) + 2c_{20}c_{21}P(\tau)P(T_c - \tau) + 2c_{12}c_{20}c_{13}c_{21}P^2(\tau) + 2c_{13}c_{12}P(\tau)P(T_c - \tau) \qquad [\text{A}]$$

Equation 16 can be calculated as

$$\zeta_{12} = c_{12}\big(b_{21}(c_{20}P(\tau) + c_{21}P(T_c - \tau))\big) + c_{13}\big(b_{21}(c_{21}P(\tau)) + b_{22}(c_{22}P(T_c - \tau))\big)$$

$$\eta_{12}^2 == E\{E[\zeta_{12}|b21, b22]\}$$

$$= \frac{(\zeta_{12}@b_{21} = b_{22} = +1) + (\zeta_{12}@b_{21} = +1, b_{22} = -1))}{2}$$

For $b_{21} = b_{22} = +1$

$$\zeta_{12} = \big(c_{12}\big(c_{20}P(\tau) + c_{21}P(T_c - \tau)\big) + c_{13}\big(c_{21}P(\tau) + c_{22}P(T_c - \tau)\big)\big)^2$$

$$= \Big(c_{12}\big(c_{20}P(\tau) + c_{21}P(T_c - \tau)\big)\Big)^2 + \Big(c_{13}\big(c_{21}P(\tau) + c_{22}P(T_c - \tau)\big)\Big)^2 + 2\Big(c_{12}\big(c_{20}P(\tau) + c_{21}P(T_c - \tau)\big)\Big)\Big(c_{13}\big(c_{21}P(\tau) + c_{22}P(T_c - \tau)\big)\Big)$$

$$= P^2(\tau) + P^2(T_c - \tau) + 2c_{20}c_{21}P(\tau)P(T_c - \tau) + P^2(\tau) + P^2(T_c - \tau)$$

For $b_{21} = +1, b_{22} = -1$

$$\zeta_{12} = \big(c_{12}\big(c_{20}P(\tau) + c_{21}P(T_c - \tau)\big) + c_{13}\big(c_{21}P(\tau) - c_{22}P(T_c - \tau)\big)\big)^2$$

$$= \big(c_{12}c_{20}P(\tau) + c_{12}c_{21}P(T_c - \tau)\big)^2 + \big(c_{13}c_{21}P(\tau) - c_{13}c_{22}P(T_c - \tau)\big)^2 + 2\big(c_{12}c_{20}P(\tau) + c_{12}c_{21}P(T_c - \tau)\big)\big(c_{13}c_{21}P(\tau) - c_{13}c_{22}P(T_c - \tau)\big)$$

$$= P(\tau) + 2c_{20}c_{21}P(\tau)P(T_c - \tau) + P(T_c - \tau) + P(\tau) - 2c_{21}c_{22}P(\tau)P(T_c - \tau)$$
$$+ P(T_c - \tau)$$
$$+ 2\big(c_{12}c_{20}c_{13}c_{21}P^2(\tau) - c_{12}c_{20}c_{13}c_{22}P(\tau)P(T_c - \tau)$$
$$+ c_{12}c_{13}P(\tau)P(T_c - \tau) - c_{12}c_{21}c_{13}c_{22}P^2(T_c - \tau)\big)$$

Thus

$$\eta_{12}^2 = \frac{(\zeta_{12}@b_{21} = b_{22} = +1) + (\zeta_{12}@b_{21} = +1, b_{22} = -1))}{2}$$

$$= 2P^2(\tau) + 2P^2(T_c - \tau) + 2c_{20}c_{21}P(\tau)P(T_c - \tau) + 2c_{12}c_{20}c_{13}c_{21}P^2(\tau)$$
$$+ 2c_{13}c_{12}P(\tau)P(T_c - \tau) \qquad [B]$$

[A] = [B] thus it is proven that Equation 13 is equivalent to Equation 15 for a special case.